Università degli Studi di Napoli *Federico II*

DOTTORATO DI RICERCA IN FISICA

Ciclo XXIX

Coordinatore: prof. Salvatore Capozziello

Microscopic multiphonon approach to spectroscopic properties of even and odd nuclei

Settore Scientifico Disciplinare FIS/04

Dottorando
Giovanni De Gregorio

Tutori
Prof. Francesco Andreozzi
Prof. Nicola Lo Iudice

Anni 2014/2017

Contents

Introduction **1**

1 Mean field approximation **4**

1.1 Independent particle model 4

1.2 Particle-hole formalism 6

1.3 HF theory 7

1.4 Hartree-Fock-Bogolyubov theory (HFB) 9

2 Tamm-Dancoff (TDA) and random-phase approximation (RPA) in the p-h basis **13**

2.1 The Hamiltonian in the j-coupled scheme 13

2.2 Tamm-Dancoff Approximation (TDA) 14

2.3 Random phase approximation (RPA) 17

3 TDA and RPA in the qp basis **20**

3.1 The Hamiltonian in the qp basis 20

3.2 TDA in the quasi-particle formalism (QTDA) 22

3.3 RPA in the quasi-particle formalism (QRPA) 23

3.4 Spurious states 24

4 The Equation of Motion Phonon Method (EMPM) 27

4.1 The EMPM in the p-h scheme 29

4.1.1 Generation of the multiphonon basis 29

4.1.2 Eigenvalue problem in the multiphonon basis 33

4.1.3 Transition Amplitudes 35

4.2 The EMPM in the quasiparticle scheme 37

4.2.1 Generation of the multiphonon basis 37

4.2.2 Eigenvalue problem in the multiphonon basis 38

4.2.3 Transition amplitudes 40

4.3 The EMPM for odd-even nuclei 41

4.3.1 Generation of the multiphonon basis 41

4.3.2 Eigenvalue problem in the multiphonon basis 43

4.3.3 Transition amplitudes 44

5 Application of the EMPM to even-even nuclei 46

5.1 Choice of the Hamiltonian 46

5.2 $E1$ response in nuclei 47

5.3 Investigation of the $E1$ response in ^{132}Sn and ^{208}Pb within the EMPM 50

5.3.1 EMPM results 51

5.4 Application of the EMPM to the neutron rich open shell ^{20}O . . . 57

6 Application of the EMPM to odd-even nuclei: ^{17}O and ^{17}F 62

6.1 Spectra 63

6.2 Moments and transitions 66

6.2.1 Magnetic moment and β-decay ft value 66

6.2.2 Electric quadrupole moments and low-lying transitions . . 68
6.2.3 Low-lying $E1$ transitions 70
6.3 Electric dipole response 71

Conclusions **79**

A HFB canonical basis **83**

B Cholesky decomposition **87**

Bibliography **88**

Introduction

Collective excitations represent one of the most distinctive features of nuclei [1]. Notable examples are the quadrupole and octupole modes which are ascribed to vibrations of the nuclear surface, or the monopole excitations (breathing mode) promoted by an isotropic compressional oscillation. These modes can have an isoscalar or isovector character according that protons and neutrons move in phase or in opposition of phase.

More peculiar is the case of the dipole mode. In fact, the isoscalar dipole operator is just proportional to the coordinate of the center of mass (CM) of the nucleus and therefore generates a spurious mode describing the excitation of the CM. Thus, in lowest order, we have only an isovector dipole mode generated by a translational oscillation of protons versus neutrons.

This oscillation gives rise to the famous giant dipole resonance (GDR). It is the first resonance discovered in nuclear systems and observed in all nuclei throughout the periodic table [2, 3]. It appears as a large hump at $E_{GDR} = 79A^{-1/3}$ of width $\Gamma \approx 5$ MeV.

Several mechanisms contribute to the total width of giant resonances in nuclei [4, 5, 6]. The first one, called Landau damping, is induced by the fragmentation of the strength into the 1particle-1hole (1p-1h) excitations of the system. Another

contribution, known as escape width, results from a direct particle emission. Finally, the spreading width is due to the coupling of the 1p-1h excitations to more complex configurations (np-nh) (n=2,3...).

The Tamm-Dancoff (TDA) and, especially, the random-phase (RPA) approximations are the most widely adopted microscopic approaches to describe collective excitations in nuclei. In both methods, the collective states are obtained as linear combinations of 1p-1h (in doubly magic nuclei) or two quasi-particle (qp) (in open shell nuclei) operators acting on an unperturbed (TDA) or correlated (RPA) ground state. By their own nature TDA and RPA, then, are able to describe only the Landau damping. They cannot account for the spreading width of the GDR or other anharmonic properties.

Several methods have been then developed to this purpose. Some of them, known as Second RPA (SRPA), couple the 1p-1h or 2 qp states to the 2p-2h or 4 qp configurations [7, 8, 9, 10, 11, 12]. This is also achieved in a relativistic approach, known as relativistic quasiparticle time blocking approximation (RTBA) [13, 14, 15]. Another variant is the particle-vibration coupling (PVC) [16, 17], where single-nucleon states couple to collective low-lying nuclear vibrations or phonons. Widely adopted is also the quasiparticle phonon model (QPM) [18], which uses a separable Hamiltonian in a multiphonon space covering up to a fraction of three RPA phonons.

Recently, an equation of motion phonon method (EMPM) [19, 20] has been proposed. The method derives and solves iteratively a set of equations of motion to generate an orthonormal basis of multiphonon states built of phonons obtained in p-h or qp TDA. Such a basis simplifies the structure of the Hamiltonian matrix and makes feasible its diagonalization in large configuration and phonon spaces.

The diagonalization produces at once the totality of eigenstates allowed by the dimensions of the multiphonon space. The formalism treats one-phonon as well as multiphonon states on the same footing, takes into account the Pauli principle, and holds for any Hamiltonian.

Recently the method has been extended to odd nuclei with one particle external to a doubly magic core. An analogous set of equations yields a basis of correlated orthonormal multiphonon particle-core states to be used for the solution of the full eigenvalue equations.

The work is organized as follows. In Chapter 1, we give a brief overview of the Hartree-Fock and Hartree-Fock-Bogolyiubov theories. TDA and RPA in the p-h basis and in the qp basis are discussed in the Chapters 2 and 3. In Chapter 4, we outline the formalism of the EMPM and the iterative procedure for generating the multiphonon basis which is used to solve the full eigenvalue equations. The method is described in the p-h scheme (first section) and in the qp formalism as well. In the last section, the extension of the EMPM to odd nuclei is discussed.

Chapters 5 and 6 are devoted to the numerical implementation of the method. Chapter 5 illustrates how the EMPM can be applied, in the p-h scheme, to the heavy neutron rich nuclei ^{132}Sn and ^{208}Sn and, in its qp version, to the neutron rich open shell ^{20}O.

Chapter 6 shows an application of the method to the odd-even nuclei ^{17}O and ^{17}F.

Concluding remarks are contained in the last chapter. The HFB canonical basis and Cholesky method for elimination of redundant basis states are discussed in the appendices.

Chapter 1

Mean field approximation

1.1 Independent particle model

The atomic nucleus can be considered a non relativistic many-body system composed of A interacting point-like nucleons described by a Hamiltonian of the form

$$H = T + V_{NN} = \sum_{i=1,A} t_i + \sum_{i<j} v(ij), \tag{1.1}$$

where $t = p^2/(2m)$ is the kinetic energy of the single nucleon and $v(ij)$ is a two-body potential. We have assumed that three-body forces can be neglected in first approximation.

The independent particle model is based on the assumption that the interaction can be absorbed to a large extent into an average one body potential U. The Hamiltonian is therefore rewritten as

$$H = H_0 + V, \tag{1.2}$$

where H_0 is an unperturbed one-body term given by

$$H_0 = \sum_{i=1,A} h_i = \sum_{i=1,A} (t_i + u_i), \tag{1.3}$$

and V is the residual two-body potential

$$V = \sum_{i<j} v(ij) - \sum_i u_i. \tag{1.4}$$

One solves first the eigenvalue equation for the Hamiltonian h_i describing the motion of the i_{th} nucleon

$$h_i \varphi_{\nu_i} = \varepsilon_{\nu_i} \varphi_{\nu_i}. \tag{1.5}$$

It is then immediate to solve the eigenvalue equations for H_0

$$H_0 \Phi_{\nu_1,\ldots\nu_i,\ldots\nu_A} = \sum_{i=i,A} \varepsilon_{\nu_i} \Phi_{\nu_1,\ldots\nu_i,\ldots\nu_A}. \tag{1.6}$$

The eigenfunctions of H_0 are just Slater determinants composed of the single particle states φ_{ν_i}

$$\Phi_{\nu_1,\ldots\nu_i,\ldots\nu_A} = \mathscr{A}\Big(\varphi_{\nu_1}\varphi_{\nu_2}\ldots\varphi_{\nu_A}\Big), \tag{1.7}$$

where $\mathscr{A}$ is is the antisymmetrizer

$$\mathscr{A} = \frac{1}{\sqrt{A!}} \sum_{\mathscr{P}} (-)^{\mathscr{P}} \mathscr{P}. \tag{1.8}$$

Here $\mathscr{P}$ is the permutation operator and $(-)^{\mathscr{P}}$ gives the parity of the permutation. The Slater determinants form an orthonormal basis in the space of A identical nucleons. This basis can be used to solve the eigenvalue problem for the full Hamiltonian H

$$H\Psi_\alpha = (H_0 + V)\Psi_\alpha = E_\alpha \Psi_\alpha. \tag{1.9}$$

The eigenfunctions are linear combinations of the basis states

$$\Psi_\alpha = \sum_{\nu_1,\ldots\nu_i,\ldots\nu_A} C^\alpha_{\nu_1,\ldots\nu_i,\ldots\nu_A} \Phi_{\nu_1,\ldots\nu_i,\ldots\nu_A}. \tag{1.10}$$

1.2 Particle-hole formalism

It is convenient to write the Hamiltonian in second quantized form. Expressed in terms of the single particle basis φ_{ν_i} H becomes

$$H = H_0 + V = \sum_{\nu} \varepsilon_{\nu} a^{\dagger}_{\nu} a_{\nu} + \frac{1}{4} \sum_{\nu_1 \nu_2 \nu_3 \nu_4} V_{\nu_1 \nu_2 \nu_3 \nu_4} a^{\dagger}_{\nu_1} a^{\dagger}_{\nu_2} a_{\nu_4} a_{\nu_3}, \tag{1.11}$$

where

$$V_{\nu_1 \nu_2 \nu_3 \nu_4} = \langle \nu_1 \nu_2 \mid V \mid \nu_3 \nu_4 \rangle - \langle \nu_1 \nu_2 \mid V \mid \nu_4 \nu_3 \rangle. \tag{1.12}$$

The operator $a^{\dagger}_{\nu}$ (a_{ν}) creates (annihilates) a particle in the state $\mid \nu \rangle = \mid \varphi_{\nu} \rangle$ with respect to the physical vacuum $\mid - \rangle$

$$a_{\nu} \mid - \rangle = 0, \tag{1.13}$$

and satisfy the anti-commutation relation

$$\{ a^{\dagger}_{\mu}, a_{\nu} \} = \delta_{\mu \nu}. \tag{1.14}$$

The Slater determinants take the form

$$\mid \nu_1, \ldots \nu_i, \ldots \nu_A \rangle = a^{\dagger}_{\nu_A} \ldots a^{\dagger}_{\nu_i} \ldots a^{\dagger}_{\nu_1} \mid - \rangle. \tag{1.15}$$

Let us consider only the unperturbed Hamiltonian H_0. Its lowest energy state, which we will denote $|\rangle$, is obtained by filling the lowest single particle orbits $\mid \nu_i \rangle$. It satisfies the eigenvalue equation

$$H_0 \mid \rangle = E^{(0)}_0 \mid \rangle, \tag{1.16}$$

with the lowest eigenvalue

$$E^{(0)}_0 = \sum_{i=1,A} \varepsilon_{\nu_i}. \tag{1.17}$$

The energy of the last filled orbit defines the Fermi energy ε_F. Let us assume that the unperturbed ground state is non degenerate. In such a case the following relations hold

$$a_p \,|\rangle = 0 \qquad \varepsilon_p > \varepsilon_F, \tag{1.18}$$

$$a_h^\dagger \,|\rangle = 0 \qquad \varepsilon_h < \varepsilon_F. \tag{1.19}$$

This property allows us to define $|\rangle$ as p-h vacuum. Thus, the particle and hole states are defined as

$$|\, p\rangle = a_p^\dagger \,|\rangle, \tag{1.20}$$

$$|\, h^{-1}\rangle = b_h^\dagger \,|\rangle = a_{\bar{h}} \,|\rangle, \tag{1.21}$$

where $\bar{h}$ denotes a time-reversed state. The excited eigenstates of H_0 have a p-h structure. The simplest ones are given by

$$H_0 \,|\, p(h)^{-1}\rangle = H_0 a_p^\dagger b_h^\dagger \,|\rangle = E_{ph} \,|\, ph^{-1}\rangle = \left[E_0^{(0)} + (\varepsilon_p - \varepsilon_h)\right] \,|\, p(h)^{-1}\rangle. \tag{1.22}$$

Thus, the excitation energy referred to the energy of the p-h vacuum is

$$\varepsilon_{ph} = E_{ph} - E_0^{(0)} = \varepsilon_p - \varepsilon_h. \tag{1.23}$$

1.3 HF theory

The independent particle model consists in neglecting the residual Hamiltonian V. It finds its theoretical justification in the Hartree-Fock (HF) theory [21, 22], which gives a rigorous prescription for deriving a mean field potential from a 2-body interaction.

Let us consider again the Hamiltonian in second quantized form

$$H = \sum_{rs} t_{rs} a_r^\dagger a_s + \frac{1}{4} \sum_{rstq} V_{rstq} a_r^\dagger a_s^\dagger a_q a_t, \tag{1.24}$$

where

$$t_{rs} = \langle s \mid T \mid r \rangle \tag{1.25}$$

are the matrix elements of the kinetic energy operator and V_{rstq} is the NN potential between antisymmetrized two-particle states defined in Eq. (1.12). The creation and annihilation operators are referred to the physical vacuum. We use the Wick's theorem and expand the two-body potential in normal order with respect to the $p-h$ vacuum. We obtain

$$H = \sum_{rs} \Big[t_{rs} + \sum_{tq} V_{rtsq} \rho_{qt} \Big] a_r^\dagger a_s - \frac{1}{2} \sum_{rstq} V_{rstq} \rho_{tr} \rho_{qs} + \frac{1}{4} \sum_{rstq} V_{rstq} : a_r^\dagger a_s^\dagger a_q a_t : . \tag{1.26}$$

The density matrix ρ is defined by

$$\rho_{rs} = \langle | \, a_s^\dagger a_r \, | \rangle, \tag{1.27}$$

where $|\rangle$ is assumed to be the HF particle-hole vacuum that has to be found. In this basis, the density matrix is diagonal

$$\rho_{rs} = \langle | \, a_s^\dagger a_r \, | \rangle = \delta_{rs} \sum_{h=1,A} \delta_{rh} \tag{1.28}$$

with eigenvalues 1 for hole states and 0 for particle states. Thus, the term in square bracket appearing in Eq. (1.26) defines the HF eigenvalue equations

$$t_{rs} + \sum_{tq} V_{rtsq} \rho_{qt} = t_{rs} + \sum_{t} V_{rtst} = \delta_{rs} \varepsilon_r. \tag{1.29}$$

In the HF basis the Hamiltonian (1.26) takes the simpler form

$$H = H_0 + V, \tag{1.30}$$

where

$$H_0 = \sum_r \varepsilon_r a_r^\dagger a_r - \frac{1}{2}\sum_{h_1 h_2} V_{h_1 h_2 h_1 h_2}, \tag{1.31}$$

and

$$V = \frac{1}{4}\sum_{rstq} V_{rstq} : a_r^\dagger a_s^\dagger a_q a_t : . \tag{1.32}$$

The HF ground state is the lowest eigenstate of H_0 with eigenvalue

$$E_0^{(0)} = \sum_{h=1,A} \varepsilon_h - \frac{1}{2}\sum_{h_1 h_2} V_{h_1 h_2 h_1 h_2}. \tag{1.33}$$

1.4 Hartree-Fock-Bogolyubov theory (HFB)

The HF description is often not completely satisfactory, especially if one deals with open-shell nuclei. The Hartree-Fock-Bogolyubov theory aims to go beyond the HF method, including explicitly the correlations introduced by the residual interaction reformulating the problem in terms of independent quasi-particles. The quasi-particle creation and annihilation operators $(\beta, \beta^\dagger)$ are related to the particle ones $(a, a^\dagger)$ through the Bogolyubov transformations

$$\beta_i^\dagger = \sum_j U_{ij} a_j^\dagger + V_{ij} a_j, \tag{1.34}$$

$$\beta_i = \sum_j U_{ij}^* a_j + V_{ij}^* a_j^\dagger, \tag{1.35}$$

that can be written in matrix form

$$\begin{pmatrix} \beta \\ \beta^\dagger \end{pmatrix} = \begin{pmatrix} U^\dagger & V^\dagger \\ V^T & U^T \end{pmatrix} \begin{pmatrix} c \\ c^\dagger \end{pmatrix} = \mathscr{W}^\dagger \begin{pmatrix} c \\ c^\dagger \end{pmatrix}, \tag{1.36}$$

where

$$\mathscr{W} = \begin{pmatrix} U & V^* \\ V & U^* \end{pmatrix}. \tag{1.37}$$

We require that the transformation preserves the commutation relations. It follows that the W matrix is unitary

$$\mathscr{W}\mathscr{W}^\dagger = \mathscr{W}^\dagger\mathscr{W} = \mathbb{I}, \tag{1.38}$$

or equivalently

$$U^\dagger U + V^\dagger V = \mathbb{I}, \qquad UU^\dagger + V^*V = \mathbb{I}, \tag{1.39}$$

$$U^T V + V^T U = 0, \qquad UV^\dagger + V^* U^T = 0. \tag{1.40}$$

The HFB ground state defines the qp vacuum $\mid 0\rangle$. Let us consider a Hamiltonian of the form

$$H = T + V, \tag{1.41}$$

its ground state expectation value

$$E_0 = \langle 0 \mid H \mid 0\rangle = \langle 0 \mid T + V \mid 0\rangle \tag{1.42}$$

is a functional of the density matrix and the paring tensor, defined respectively by

$$\rho_{sr} = \langle 0 \mid a_r^\dagger a_s \mid 0\rangle, \qquad \kappa_{sr} = \langle 0 \mid a_r a_s \mid 0\rangle, \tag{1.43}$$

which can be written in terms of U and V matrices as

$$\rho = V^* V^T, \qquad \kappa = V^* U^T. \tag{1.44}$$

Using the variational principle [23] we minimize E_0 with the constraint

$$tr\rho = N, \tag{1.45}$$

ensuring that the number of particle is conserved on average. We obtain

$$\sum_{rs} \frac{\delta E_0}{\delta V_{rs}^*} \delta V_{rs}^* + \frac{\delta E_0}{\delta U_{rs}^*} \delta U_{rs}^* = 0. \tag{1.46}$$

This variation leads to an equation that can be written in matrix form

$$\begin{pmatrix} h-\lambda & \Delta \\ \Delta^\dagger & -h+\lambda \end{pmatrix} \begin{pmatrix} V \\ U \end{pmatrix} = E \begin{pmatrix} V \\ U \end{pmatrix}, \tag{1.47}$$

where

$$(h-\lambda)_{rs} = h_{rs} - \lambda\,\delta_{rs} = t_{rs} + \sum_{kl} V_{rstq}\rho_{qt} - \lambda\,\delta_{rs}, \tag{1.48}$$

$$\Delta_{rs} = \frac{1}{4}\sum_{kl} V_{tqsr}\kappa_{qt}^\dagger. \tag{1.49}$$

For practical purposes it is convenient to adopt the canonical basis (App. A). As shown in [24], in such a basis the Bogolyubov transformations become the canonical one (A.8), while the density matrix ρ and the pairing tensor κ take the simple form

$$\rho = \begin{pmatrix} v_r^2 & 0 \\ 0 & v_r^2 \end{pmatrix}, \qquad \kappa = \begin{pmatrix} 0 & u_r v_r \\ -u_r v_r & 0 \end{pmatrix}, \tag{1.50}$$

with the condition (1.39) that becomes

$$u_r^2 + v_r^2 = 1. \tag{1.51}$$

We can therefore derive

$$u_r^2 = \frac{1}{2}\left(1 - \frac{h_{rr}-\lambda}{E_r}\right), \qquad v_r^2 = \frac{1}{2}\left(1 + \frac{h_{rr}-\lambda}{\sqrt{E_r}}\right), \tag{1.52}$$

where

$$E_r = \sqrt{(h_{rr}-\lambda)^2 + \Delta_{rr}^2} \tag{1.53}$$

is the qp energy and

$$h_{rr} = t_{rr} + \sum_{kl} V_{rsrs} v_r^2, \tag{1.54}$$

$$\Delta_{rr} = \frac{1}{4} \sum_{s} V_{r\bar{r}s\bar{s}} u_s v_s. \tag{1.55}$$

The chemical potential λ is fixed by the number conserving condition which in the canonical basis becomes

$$\sum_r v_r^2 = N. \tag{1.56}$$

It is to be pointed out that the quasi-particle energies E_r do not coincide in general with the HFB eigenvalues E obtained by solving the Eqs. (1.47).

Chapter 2

Tamm-Dancoff (TDA) and random-phase approximation (RPA) in the p-h basis

The Tamm-Dancoff (TDA) and the random-phase approximation (RPA) are the simplest and most widely adopted approaches to study nuclear excitations. We will derive the equations in the j-coupled scheme starting from the HF approximation for the ground state.

2.1 The Hamiltonian in the j-coupled scheme

Let us consider the Hamiltonian

$$H = H_0 + V, \tag{2.1}$$

in the j-coupled scheme the unperturbed part is given by

$$H_0 = \sum_{rs} [r]^{1/2} t_{rs} \left[a_r^\dagger \times b_s \right]^0, \tag{2.2}$$

where $[r] = (2j_r + 1)$, and $[.. \times ..]^J$ denotes the coupling to spin J defined by

$$\left[a_r^\dagger \times b_s \right]_M^J = \sum_{m_r m_s} \langle j_r m_r j_s m_s | JM \rangle a^\dagger_{n_r l_r j_r m_r} b_{n_s l_s j_s m_s}, \tag{2.3}$$

with

$$b_s = b_{n_s l_s j_s m_s} = (-1)^{j_s + m_s} a_{n_s l_s j_s - m_s}, \tag{2.4}$$

and the potential takes the form

$$V = -\frac{1}{4} \sum_{rstq} [\Omega]^{1/2} V^\Omega_{rstq} \left[\left[a_r^\dagger \times a_s^\dagger \right]^\Omega \times \left[b_t \times b_q \right]^\Omega \right]^0. \tag{2.5}$$

It is useful for our purposes to write the two-body potential in the recoupled form

$$V = \frac{1}{4} \sum_{rstq\sigma} [\sigma]^{\frac{1}{2}} F^\sigma_{rstq} \left[\left[a_r^\dagger \times b_t \right]^\sigma \times \left[a_s^\dagger \times b_q \right]^\sigma \right]^0 - \sum_{rsq} [q]^{\frac{1}{2}} F^0_{rsqq} \left[a_r^\dagger \times b_s \right]^0, \tag{2.6}$$

obtained by the use of the Pandya transformation

$$F^\sigma_{rstq} = \sum_\Omega (-1)^{r+q-\sigma-\Omega} W(rstq; \Omega\sigma) V^\Omega_{rstq}, \tag{2.7}$$

where $W(rstq; \Omega\sigma)$ are Racah coefficients.

2.2 Tamm-Dancoff Approximation (TDA)

The Tamm-Dancoff Approximation is the easiest microscopic treatment of nuclear excitations for closed shell nuclei. It diagonalizes the nuclear Hamiltonian in a space spanned by the 1p-1h configurations

$$| \left(p \times h^{-1} \right)^\lambda \rangle = \left(a_p^\dagger \times b_h \right)^\lambda | \rangle. \tag{2.8}$$

Let consider the Hamiltonian

$$H = H_0 + V, \tag{2.9}$$

where

$$H_0 = \sum_r [r]^{1/2} \varepsilon_r \left(a_r^\dagger \times b_r \right)^0, \tag{2.10}$$

and

$$V = \frac{1}{4} \sum_{rstqJ} [\sigma]^{1/2} F^\sigma_{rstq} \left[\left(a_r^\dagger \times b_t \right)^\sigma \times \left(a_s^\dagger \times b_q \right)^\sigma \right]^0. \tag{2.11}$$

We intend to solve the equation

$$\langle (p \times h^{-1})^\lambda \mid H \mid \lambda \rangle = E_\lambda \langle (p \times h^{-1})^\lambda \mid \lambda \rangle = E_\lambda C^\lambda_{ph}, \tag{2.12}$$

or the equivalent one

$$\langle \mid \overline{\left[(a_p^\dagger \times b_h)^\lambda, H \right]}^\lambda \mid \lambda \rangle = (E_\lambda - E_0) \langle \mid \overline{(a_p^\dagger \times b_h)^\lambda} \mid \lambda \rangle = \omega_\lambda C^\lambda_{ph}. \tag{2.13}$$

After expanding the commutator in the left-hand member of the above equation we get

$$\sum_{p'h'} A^\lambda(ph, p'h') C^\lambda_{p'h'} = \omega_\lambda C^\lambda_{ph}, \tag{2.14}$$

where

$$A^\lambda(ph, p'h') = (\varepsilon_p - \varepsilon_h)\delta_{pp'}\delta_{hh'} + (-)^{p-h+\lambda} F^\lambda_{hpp'h'} \tag{2.15}$$

is the TDA matrix. A graphical representation of the interaction is shown in Fig.(2.1).

The solution of the TDA eigenvalue equation (2.14) yields the eigenvectors

$$\mid \lambda \rangle = \sum_{ph} C^\lambda_{ph} \mid (p \times h^{-1})^\lambda \rangle = O^\dagger_\lambda \mid \rangle, \tag{2.16}$$

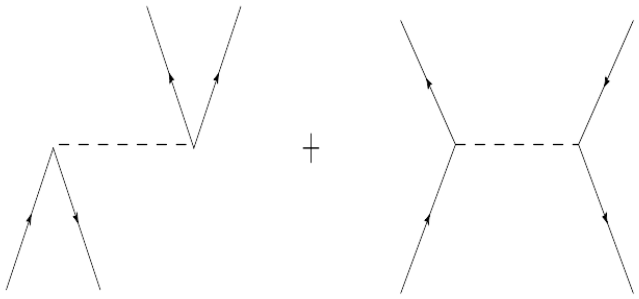

Figure 2.1: TDA vertices

where $O^{\dagger}_{\lambda}$ is the phonon operator

$$O^{\dagger}_{\lambda} = \sum_{ph} (a^{\dagger}_{p} \times b_{h})^{\lambda}. \tag{2.17}$$

A diagrammatic representation of the TDA phonons is illustrated in Fig. (2.2).

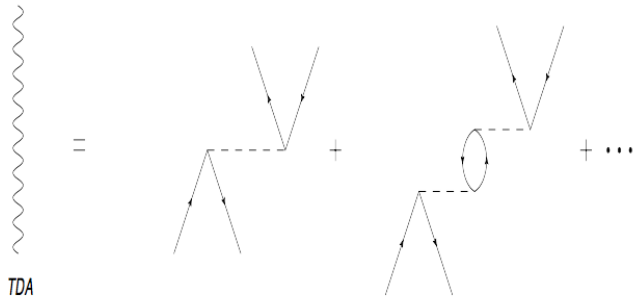

Figure 2.2: TDA series

In the coupled scheme, the one-body operator has the form

$$\mathscr{M}(\lambda) = \frac{1}{[\lambda]^{1/2}} \sum_{rs} \langle r \parallel \mathscr{M}_{\lambda} \parallel s \rangle \left[a^{\dagger}_{r} \times b_{s} \right]^{\lambda}, \tag{2.18}$$

and the transition amplitudes are given by

$$\langle \lambda \parallel \mathscr{M}(\lambda) \parallel \rangle = \sum_{ph} C^{\lambda}_{ph} \langle p \parallel \mathscr{M}_{\lambda} \parallel h \rangle. \tag{2.19}$$

2.3 Random phase approximation (RPA)

The RPA approximation, unlike TDA, takes into account the ground state correlations. Therefore the p-h operator is of the general form

$$O^{\dagger}_{\lambda} = \sum_{ph} \left[C^{\lambda}_{ph} Z^{\lambda}_{ph} + D^{\lambda}_{ph} \overline{Z}^{\lambda}_{ph} \right], \tag{2.20}$$

where

$$Z^{\lambda}_{ph} = \left(a^{\dagger}_{p} \times b_{h} \right)^{\lambda}, \qquad \overline{Z}^{\lambda}_{ph} = - \left(b^{\dagger}_{h} \times a_{p} \right)^{\lambda}. \tag{2.21}$$

The above equations show that a p-h state can be generated either by creating or destroying a p-h pair from the correlated ground state (Fig. 2.3).

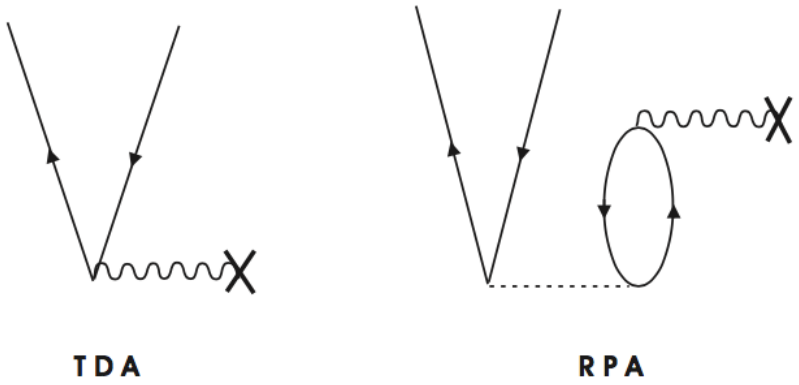

Figure 2.3: RPA excitation mechanisms

The eigenvalue equations are obtained by solving

$$\langle RPA \mid \left[\overline{Z}^{\lambda}_{ph}, \left[H, O^{\dagger}_{\lambda} \right]^{\lambda} \right]^{0} \mid RPA \rangle = \omega_{\lambda} \langle RPA \mid \left[\overline{Z}^{\lambda}_{ph}, O^{\dagger}_{\lambda} \right]^{0} \mid RPA \rangle, \tag{2.22}$$

$$\langle RPA \mid \left[Z^{\lambda}_{ph}, \left[H, O^{\dagger}_{\lambda} \right]^{\lambda} \right]^{0} \mid RPA \rangle = \omega_{\lambda} \langle RPA \mid \left[Z^{\lambda}_{ph}, O^{\dagger}_{\lambda} \right]^{0} \mid RPA \rangle, \tag{2.23}$$

where $\omega_\lambda = E_\lambda - E_0$, and $\mid RPA\rangle$ is the RPA ground state defined by

$$O_\lambda \mid RPA\rangle = 0. \tag{2.24}$$

It is convenient to put the eigenvalue equations in matrix form

$$\begin{pmatrix} A^\lambda & B^\lambda \\ -B^{\lambda *} & -A^{\lambda *} \end{pmatrix} \begin{pmatrix} C^\lambda \\ D_\lambda \end{pmatrix} = \omega_\lambda \begin{pmatrix} C^\lambda \\ D_\lambda \end{pmatrix}, \tag{2.25}$$

with A, B defined as

$$A = [\lambda]^{-1/2} \langle RPA \parallel \left[\overline{Z}^\lambda_{ph}, \left[H, Z^\lambda_{ph}\right]^\lambda\right]^0 \parallel RPA\rangle, \tag{2.26}$$

$$B = [\lambda]^{-1/2} \langle RPA \parallel \left[\overline{Z}^\lambda_{ph}, \left[H, \overline{Z}^\lambda_{ph}\right]^\lambda\right]^0 \parallel RPA\rangle. \tag{2.27}$$

The A and B matrix are computed in the quasi-boson approximation. It consists in replacing the correlated ground state with the unperturbed HF one. This approximation relies on the assumption that the RPA ground state does not differ very much from the unperturbed p-h vacuum. One obtains

$$A \approx [\lambda]^{-1/2} \langle \parallel \left[\overline{Z}^\lambda_{ph}, \left[H, Z^\lambda_{ph}\right]^\lambda\right]^0 \parallel \rangle = (\varepsilon_p - \varepsilon_h)\delta_{pp'}\delta_{hh'} + (-)^{p-h+\lambda} F^\lambda_{hpp'h'} \tag{2.28}$$

$$B \approx [\lambda]^{-1/2} \langle \parallel \left[\overline{Z}^\lambda_{ph}, \left[H, \overline{Z}^\lambda_{ph}\right]^\lambda\right]^0 \parallel \rangle = F^\lambda_{php'h'}. \tag{2.29}$$

The block-diagonal matrix A is the TDA matrix (2.14). The off-diagonal block B takes into account the correlation of the ground state. This is represented by the diagram in Fig. (2.4).

The solution of the above RPA equations gives the eigenvectors

$$\mid \lambda\rangle = O^\dagger_\lambda \mid \rangle. \tag{2.30}$$

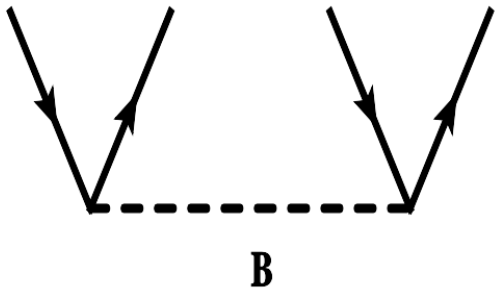

Figure 2.4: Diagrammatic representation of B

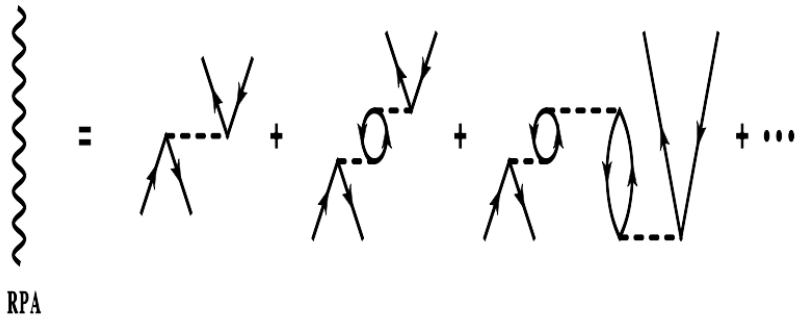

Figure 2.5: RPA series

A diagrammatic representation of the RPA phonons is illustrated in Fig. (2.5).

The transition amplitudes of the multipole operator (2.18) are

$$\langle \lambda \,||\, \mathscr{M}_\lambda \,||\, \rangle = \sum_{p\leq h} \langle p \,||\, \mathscr{M}_\lambda \,||\, h \rangle \left[C_{ph}^{\lambda *} - (-1)^\lambda D_{ph}^{\lambda *} \right]. \tag{2.31}$$

Chapter 3

TDA and RPA in the qp basis

In this chapter we will derive the TDA and RPA equation in the qp basis for describing the excitations of open shell nuclei.

3.1 The Hamiltonian in the qp basis

When the Hamiltonian (2.1) is expressed in terms of the canonical *qp* operators (A.8) takes the form

$$H = E_0 + H_{11} + V_{res}, \tag{3.1}$$

where E_0 is the HFB ground state

$$E_0 = \sum_r [r] t_{rr} v_r^2 + \frac{1}{2} \sum_r [r] \left(\Gamma_{rr} v_r^2 + \Delta_{rr} u_r v_r \right), \tag{3.2}$$

and

$$\Gamma_{rs} = [r]^{-1/2} \sum_t F^0_{rstt} \langle 0 \mid (a_t^\dagger \times a_t)^0 \mid 0 \rangle = [r]^{-1/2} \sum_t [t]^{1/2} F^0_{rstt} v_t^2, \tag{3.3}$$

$$\Delta_{rs} = -\frac{1}{2} [r]^{-1/2} \sum_t V^0_{rstt} \langle 0 \mid (a_t \times a_t)^0 \mid 0 \rangle = \frac{1}{2} [r]^{-1/2} \sum_t [t]^{1/2} V^0_{rstt} u_t v_t, \tag{3.4}$$

are the Hartree-Fock and pairing potentials, respectively. The one-body qp Hamiltonian has the expression

$$H_{11} = \sum_{rs} [r]^{1/2} \mathscr{E}_{rs} \left[\alpha_r^\dagger \times \alpha_s \right]^0, \tag{3.5}$$

where

$$\mathscr{E}_{rs} = (\varepsilon_{rs} - \lambda \delta_{rs})(u_r u_s - v_r v_s) + \Delta_{rs}(u_r v_s + v_r u_s), \tag{3.6}$$

with

$$\varepsilon_{rs} = t_{rs} + \Gamma_{rs}. \tag{3.7}$$

It has to be noticed that the H_{11} is non diagonal as it would be the case if computed in the HFB basis. The residual two-body potential describes the interaction among quasi-particles and has the composite form

$$V_{res} = V_{22} + V_{31} + V_{40} + V_{13} + V_{04}, \tag{3.8}$$

where V_{ij} are expressed in term of i creation and j annihilation qp operators and V_{ji} are che Hermitian conjugate of V_{ij}. They are defined by

$$V_{22} = -\sum_{r\le s}^{\sigma} \sum_{t\le q} [\sigma]^{1/2} \zeta_{rs}^2 \zeta_{tq}^2 V_{rstq}^{\sigma}(22) \left[(\alpha_r^\dagger \times \alpha_s^\dagger)^\sigma \times (\alpha_t \times \alpha_q)^\sigma \right]^0, \tag{3.9}$$

$$V_{31} = \frac{1}{2} \sum_{(r\le s)}^{\sigma} \sum_{tq} [\sigma]^{1/2} \zeta_{rs}^2 V_{rstq}^{\sigma}(31) \left[(\alpha_r^\dagger \times \alpha_s^\dagger)^\sigma \times (\alpha_t^\dagger \times \alpha_q)^\sigma \right]^0, \tag{3.10}$$

$$V_{40} = -\sum_{(r\le s)}^{\sigma} \sum_{t\le q} [\sigma]^{1/2} \zeta_{rs}^2 \zeta_{tq}^2 V_{rstq}^{\sigma}(40) \left[(\alpha_r^\dagger \times \alpha_s^\dagger)^\sigma \times (\alpha_t^\dagger \times \alpha_q^\dagger)^\sigma \right]^0, \tag{3.11}$$

where $\zeta_{rs} = (1+\delta_{rs})^{-1/2}$, and

$$\begin{aligned} V_{rstq}^{\sigma}(22) = \big[& V_{rstq}^{\sigma}(u_r u_s u_t u_q + v_r v_s v_t v_q) + F_{rstq}^{\sigma}(u_r v_s v_t u_q + v_r u_s u_t v_q) + \\ & (-)^{r-s-\sigma} F_{srtq}^{\sigma}(v_r u_s v_t u_q + u_r v_s u_t v_q) \big], \end{aligned} \tag{3.12}$$

$$V^{\sigma}_{rstq}(31) = \left[F^{\sigma}_{rstq}(u_r v_s u_t u_q + v_r u_s v_t v_q) - (-)^{r-s-\sigma} F^{\sigma}_{rstq}(v_r u_s u_t u_q - u_r v_s v_t v_q)\right], \tag{3.13}$$

$$V^{\sigma}_{rstq}(40) = \left[F^{\sigma}_{rstq}(u_r v_s u_t v_q + v_r u_s v_t u_q) - (-)^{r-s-\sigma} F^{\sigma}_{rsqt}(u_r v_s v_t u_q + v_r u_s u_t v_q)\right]. \tag{3.14}$$

3.2 TDA in the quasi-particle formalism (QTDA)

In the qp scheme we use the basis ($r \leq s$)

$$\mid (r \times s)^{\lambda}\rangle = Z^{\lambda}_{rs} \mid 0\rangle, \tag{3.15}$$

where

$$Z^{\lambda}_{rs} = -\zeta_{rs}(\alpha^{\dagger}_r \times \alpha^{\dagger}_s)^{\lambda}, \tag{3.16}$$

with the Hamiltonian of the form given by (3.1). In close analogy with the p-h derivation we have to solve the eigenvalue equation

$$\langle 0 \parallel \left[\overline{Z}^{\lambda}_{rs}, H\right]^{\lambda} \parallel \lambda\rangle = \omega_{\lambda} \langle 0 \parallel \overline{Z}^{\lambda}_{rs} \parallel \lambda\rangle. \tag{3.17}$$

After expanding the commutator we get

$$\sum_{t\leq q} A^{\lambda}(rs,tq) C^{\lambda}_{tq} = \omega_{\lambda} C^{\lambda}_{rs}, \tag{3.18}$$

where the A matrix is given by

$$A^{\lambda}(rs,tq) = \zeta_{rs}\zeta_{tq}\left[H_{rstq}(11) + V_{rstq}(22)\right]. \tag{3.19}$$

The first term is

$$H_{rstq}(11) = \delta_{sq}\mathscr{E}_{rt} + \delta_{rt}\mathscr{E}_{sq} - (-)^{r+s-\lambda}[\delta_{st}\mathscr{E}_{rq} + \delta_{rq}\mathscr{E}_{st}]. \tag{3.20}$$

The second term is the two-body matrix element given by the Eq (3.12). Eq. shows that the one-body matrix element is non-diagonal in the canonical HFB basis. The solution of the eigenvalue equation yields the eigenvectors

$$\mid \lambda\rangle = \sum_{rs} C^{\lambda}_{rs} \mid (r\times s)^{\lambda}\rangle = O^{\dagger}_{\lambda} \mid 0\rangle \tag{3.21}$$

where

$$O^{\dagger}_{\lambda} = \sum_{rs} \zeta_{rs} C^{\lambda}_{rs} \left(\alpha^{\dagger}_{r} \times \alpha^{\dagger}_{s}\right) \tag{3.22}$$

are the QTDA phonons of energies ω_{λ}.

The transition amplitudes of a general multipole operator are

$$\langle \lambda \mid\mid \mathscr{M}_{\lambda} \mid\mid 0\rangle = \sum_{r\leq s} C^{*\lambda}_{rs} \zeta_{rs} \left(u_r v_s + (-)^{\lambda} v_r u_s\right) \langle r \mid\mid \mathscr{M}_{\lambda} \mid\mid s\rangle. \tag{3.23}$$

3.3 RPA in the quasi-particle formalism (QRPA)

The QRPA creation operator is

$$O^{\dagger}_{\lambda} \;=\; \sum_{ph} \left[C^{\lambda}_{ph} Z^{\lambda}_{ph} + D^{\lambda}_{ph} \overline{Z}^{\lambda}_{ph}\right], \tag{3.24}$$

where

$$Z^{\lambda}_{ph} = \zeta_{rs} \left(\alpha^{\dagger}_{r} \times \alpha^{\dagger}_{s}\right)^{\lambda}, \qquad \overline{Z}^{\lambda}_{ph} = -\zeta_{rs} \left(\alpha_{r} \times \alpha_{s}\right)^{\lambda}. \tag{3.25}$$

The QRPA eigenvalue equations, in analogy with the p-h derivation, can be written in matrix form

$$\begin{pmatrix} A^{\lambda} & B^{\lambda} \\ -B^{\lambda *} & -A^{\lambda *} \end{pmatrix} \begin{pmatrix} C^{\lambda} \\ D_{\lambda} \end{pmatrix} = \omega_{\lambda} \begin{pmatrix} C^{\lambda} \\ D_{\lambda} \end{pmatrix}, \tag{3.26}$$

where $\omega_{\lambda} = E_{\lambda} - E_0$. The block matrices are defined as

$$A = [\lambda]^{-1/2} \langle 0 \parallel \left[\overline{Z}^{\lambda}_{ph}, \left[H, Z^{\lambda}_{ph}\right]^{\lambda}\right]^{0} \parallel 0\rangle, \tag{3.27}$$

$$B = [\lambda]^{-1/2}\langle 0 \parallel \left[\overline{Z}^{\lambda}_{ph}, \left[H, \overline{Z}^{\lambda}_{ph}\right]^{\lambda}\right]^{0} \parallel 0\rangle. \tag{3.28}$$

The block-diagonal matrix A is just the QTDA matrix (Eq. 3.19). The off-diagonal block takes into account the correlation of the ground state and is given by

$$\begin{aligned} B^{\lambda}(rs,tq) &= \zeta_{rs}\zeta_{tq}V^{\lambda}_{rstq}[u_r u_s v_t v_q + u_t u_q v_r v_s] - \zeta_{rs}\zeta_{tq}\left(F^{\lambda}_{rstq}[u_r v_s u_t v_q + u_s v_r u_q v_t]\right. \\ &- \left.(-)^{t+q-\lambda}F^{\lambda}_{rstq}[u_r v_s u_q v_t + u_s v_r u_t v_q\right). \end{aligned} \tag{3.29}$$

The transition amplitudes for a generic multipole operator are

$$\langle \lambda \parallel \mathscr{M}_{\lambda} \parallel 0\rangle = \sum_{r\leq s}\langle r \parallel \mathscr{M}_{\lambda} \parallel s\rangle \zeta_{rs}\left[u_r v_s + (-1)^{\lambda}u_s v_r\right]\left[C^{\lambda *}_{rs} - (-1)^{\lambda}D^{\lambda *}_{rs}\right]. \tag{3.30}$$

3.4 Spurious states

In a fully self-consistent QRPA calculation the 1^- and 0^+ spurious states lie at zero excitation energy and collect the total strength induced by the CM and the number operators respectively. Numerically, their complete decoupling from the physical intrinsic states is achieved if a sufficiently large configuration space is adopted. This was the case of Ref. [25], where 15 major oscillator shells were considered in order to generate the HFB basis.

In our QTDA calculations, as shown in Ref. [26], this complete separation is not achieved, and the spurious admixtures induced by the center-of-mass motion and the violation of the particle number contaminate the spectra. We eliminate completely and exactly these spurious admixtures by resorting to the Gramm-

Schmidt orthogonalization procedure. Let the spurious state be

$$\mid \Phi_0\rangle = \frac{1}{N(1)} \sum_{i=1}^{n} C_i \mid i\rangle \tag{3.31}$$

where

$$N^2(1) = \sum_{i=1}^{n} \mid C_i \mid^2 \tag{3.32}$$

is the normalization constant. The orthogonalized states have the expression

$$\mid \Phi_{k-1}\rangle = \frac{1}{N(k-1)N(k)} \left[N^2(k-1) \mid k-1\rangle - \sum_{i=k,n} C_{k-1}C_i \mid i\rangle \right], \tag{3.33}$$

where (k=2,3,...n)

$$N^2(k) = \sum_{i=k,n} \mid C_i \mid^2 . \tag{3.34}$$

For $k = n$ the sum disappear. So we have simply

$$\Phi_{n-1} = \frac{1}{N(n-1)N(n)} \left[N^2(n-1) \mid n-1\rangle - C_{n-1}C_n \mid n\rangle \right], \tag{3.35}$$

where

$$N^2(n) = \mid C_n \mid^2 . \tag{3.36}$$

The CM spurious state $\left(\lambda_1 = (\kappa_1, 1^-)\right)$ is

$$\mid \lambda_1\rangle = \frac{1}{N_1} R_\mu \mid 0\rangle, \tag{3.37}$$

where R_μ is the CM coordinate and N_1 the normalization constant. Expanded in the two quasi-particle basis states, it acquires the structure

$$\mid \lambda_1\rangle = \frac{1}{N_1} R_\mu \mid 0\rangle = \frac{1}{N_1} \sum_{r \leq s} C_{rs}^{\lambda_1} \mid (r \times s)^{1^-}\rangle, \tag{3.38}$$

where $C_{rs}^{\lambda_1}$ are the unnormalized coefficients

$$C_{rs}^{\lambda_1} = \sqrt{\frac{4\pi}{9}} \frac{1}{A} \langle r \mid\mid rY_1 \mid\mid s\rangle (u_r v_s - u_s v_r), \tag{3.39}$$

and the normalization coefficient is given by

$$N_1^2 = \sum_{r \leq s} \mid C_{rs}^{\lambda_1} \mid^2 . \tag{3.40}$$

Similarly, the number operator spurious state ($\lambda_0 = (\kappa_0, 0^+)$) is obtained by applying the number operator in normal order to the HFB vacuum. We get

$$\mid \lambda_0 \rangle = \frac{1}{N_0} \sum_r C_{rr}^{\lambda_0} \mid (r \times s)^{0^+} \rangle, \tag{3.41}$$

where

$$C_{rs}^{\lambda_0} = \sqrt{2[r]} u_r v_r, \tag{3.42}$$

and

$$N_0^2 = \sum_r \mid C_{rr}^{\lambda_0} \mid^2 . \tag{3.43}$$

Applying such a procedure to the $J^\pi = 1^-$ and $J^\pi = 0^+$ states we determine the basis states orthogonal to $\mid \lambda_1 \rangle$ and $\mid \lambda_0 \rangle$. The obtained states, which are linear combinations of the p-h states or qp states, must be used to construct and diagonalize the Hamiltonian matrix, yielding eigenstates rigorously free of spurious admixtures.

Chapter 4

The Equation of Motion Phonon Method (EMPM)

TDA and RPA account only for the 1p-1h fragmentation ("Landau damping"). In order to try to reproduce the spreading width it is necessary to couple this mode to more complex configurations (2p-2h, 3p-3h,...) as done in several extension of RPA.

The most common extension is known as second RPA (SRPA) and couples the particle-hole (ph) or quasiparticle (qp) RPA modes to the 2p-2h or 4qp configurations. The SRPA equations were first derived by Sawicki [7] and later by Yannouleas et al. [8, 9].

Several SRPA calculations were performed employing different potentials. Some adopted realistic NN interactions, as Roth and coworkers [10], which have adopted an effective interaction derived from the Argonne V18 potential using the unitary correlation operator method (UCOM). Others have used phenomenological potentials like Gogny [12] or Skyrme [27, 28]. A Skyrme interaction has been

used also in Ref. [29] within a second TDA (STDA) approach.

A density dependent zero-range interaction was adopted in a linear response function approach to diagonalize the residual interaction in the combined 1p-1h and 2p-2h subspaces [30, 31].

Of phenomenological nature is also the core-coupling RPA model using the density dependent Migdal δ-function force with parameters fitted in the Pb region to electromagnetic properties [32]. In an analogous calculation, using a Skyrme interaction, the single particle states were coupled to the surface modes generated within RPA [33].

The quasiparticle-phonon model (QPM) [34] adopts a two-body Hamiltonian of separable form in a multiphonon space covering up to a fraction of three RPA phonons. QPM calculations have been performed to study the pygmy resonance [35, 36, 37, 38, 39] and the fine structure of the giant M1 resonance [40].

The relativistic quasiparticle time blocking approximation (RTBA) [41], framed within a covariant EDF theory, couples two-quasiparticle states to collective vibrations. It has been adopted to investigate the electric dipole response [42, 13, 43, 14, 15] and the Gamow-Teller transitions [44].

Anharmonic effects have been studied recently also within an equation of motion phonon method (EMPM)[19, 45]. This derives and solves iteratively a set of equations of motion to generate an orthonormal basis of multiphonon states built of phonons obtained in particle-hole (p-h) or quasiparticle TDA. Such a basis simplifies the structure of the Hamiltonian matrix and makes feasible its diagonalization in large configuration and phonon spaces.

The method has been applied mainly to the heavy neutron rich closed shell nuclei ^{132}Sn and ^{208}Pb [46, 47], and in the qp scheme to the neutron rich open

shell ^{20}O [48].

4.1 The EMPM in the p-h scheme

4.1.1 Generation of the multiphonon basis

The primary goal of the method is to generate an orthonormal n-phonon basis of the form

$$|\beta_n >= \sum_{\lambda \alpha_{n-1}} C^{\beta_n}_{\lambda \alpha_{n-1}} \mid (\lambda \times \alpha_{n-1})^{\beta} \rangle = \sum_{\lambda \alpha_{n-1}} C^{\beta_n}_{\lambda \alpha_{n-1}} \left\{ O^{\dagger}_{\lambda} \times \mid \alpha_{n-1} \rangle \right\}^{\beta}, \quad (4.1)$$

where $O^{\dagger}_{\lambda}$ is the TDA phonon operator given by

$$O^{\dagger}_{\lambda} = \sum_{ph} C^{\lambda}_{ph} \left(a^{\dagger}_{p} \times b_{h} \right)^{\lambda}. \quad (4.2)$$

It acts on the $(n-1)$-phonon basis states $\mid \alpha_{n-1} \rangle$, assumed to be known.

The eigenvalue equation are derived from

$$\langle \beta \mid H \mid (\lambda \times \alpha)^{\beta} \rangle = E_{\beta} \langle \beta \mid (\lambda \times \alpha)^{\beta} \rangle, \quad (4.3)$$

where the n subscript has been omitted and will be used when necessary. We start with the equation of motion

$$\langle \beta \mid \left(\left[H, O^{\dagger}_{\lambda} \right]^{\lambda} \times \mid \alpha \rangle \right)^{\beta} = \left(E_{\beta} - E_{\alpha} \right) \langle \beta \mid (\lambda \times \alpha)^{\beta} \rangle. \quad (4.4)$$

Upon applying the Wigner-Eckart theorem, we obtain the equivalent equations

$$\langle \beta \parallel \left[H, O^{\dagger}_{\lambda} \right]^{\lambda} \parallel \alpha \rangle = \left(E_{\beta} - E_{\alpha} \right) X^{\beta}_{\lambda \alpha}, \quad (4.5)$$

where

$$X^{\beta}_{\lambda \alpha} = \langle \beta \parallel O^{\dagger}_{\lambda} \parallel \alpha \rangle. \quad (4.6)$$

The quantities $C^{\beta}_{\lambda\alpha}$ and $X^{\beta}_{\lambda\alpha}$ satisfy the normalization condition

$$1 = \langle \beta \mid \beta \rangle = [\beta]^{-1/2} \sum_{\lambda\alpha} X^{\beta}_{\lambda\alpha} C^{\beta}_{\lambda\alpha}, \tag{4.7}$$

and are related by

$$X^{\beta}_{\lambda\alpha} = \sum_{\lambda'\alpha'} \mathscr{D}^{\beta}_{\lambda\alpha,\lambda'\alpha'} C^{\beta}_{\lambda'\alpha'}. \tag{4.8}$$

Here $\mathscr{D}^{\beta}_{\lambda\alpha,\lambda'\alpha'}$ is the overlap or metric matrix which reintroduces the exchange terms among different phonons and, therefore, re-establishes the Pauli principle. It is given by

$$\begin{aligned} \mathscr{D}^{\beta}(\lambda\alpha;\lambda'\alpha') = \langle (\lambda\times\alpha)^{\beta} \mid (\lambda'\times\alpha')^{\beta} \rangle = \\ \delta_{\lambda\lambda'}\delta_{\alpha\alpha'} + \sum_{\gamma} W(\lambda\alpha\alpha'\lambda';\beta\gamma) X^{\alpha}_{\gamma\lambda'}(n-1) X^{\alpha'}_{\gamma\lambda}(n-1) \\ -(-)^{\lambda+\alpha-\beta} \sum_{rs\sigma} W(\lambda\alpha\lambda'\alpha';\beta\sigma) \rho_{\lambda'\lambda}([r\times s]^{\sigma}) \rho_{\alpha\alpha'}([r\times s]^{\sigma}), \end{aligned} \tag{4.9}$$

where the phonon densities are

$$\begin{aligned} \rho_{\alpha\alpha'}([r\times s]^{\sigma}) = \langle \alpha \parallel \left[a^{\dagger}_{r} \times b_{s} \right]^{\sigma} \parallel \alpha' \rangle \\ = \sum_{\lambda\lambda'} \rho_{\lambda\lambda'}\left([r\times s]^{\sigma}\right) R^{(\sigma)}_{\lambda\lambda'}\left(\alpha\alpha'\right) + \sum_{\gamma\gamma'} \rho^{(n-1)}_{\gamma\gamma'}\left([r\times s]^{\sigma}\right) R^{(\sigma)}_{\gamma\gamma'}\left(\alpha\alpha'\right). \end{aligned} \tag{4.10}$$

Here $(r = p, s = p')$ or $(r = h, s = h')$ and

$$R^{(\sigma)}_{\lambda\lambda'}\left(\alpha\alpha'\right) = [\alpha]^{1/2} \sum_{\gamma} W(\alpha'\sigma\gamma\lambda;\alpha\lambda') C^{\alpha}_{\lambda\gamma}(n) X^{\alpha'}_{\lambda'\gamma}(n), \tag{4.11}$$

$$R^{(\sigma)}_{\gamma\gamma'}\left(\alpha\alpha'\right) = [\alpha]^{1/2} \sum_{\lambda} W(\alpha'\sigma\lambda\gamma;\alpha\gamma') C^{\alpha}_{\lambda\gamma}(n) X^{\alpha'}_{\lambda\gamma'}(n). \tag{4.12}$$

After expanding the commutator and expressing the p-h operators in terms of the phonon operator $O^{\dagger}_{\lambda}$ upon inversion of Eq. (4.2), we obtain

$$\sum_{\lambda'\alpha'} \mathscr{A}^{\beta}_{\lambda\alpha,\lambda'\alpha'} X^{\beta}_{\lambda'\alpha'} = E_{\beta} X^{\beta}_{\lambda\alpha}. \tag{4.13}$$

The $\mathscr{A}$ matrix has the simple structure

$$\mathscr{A}^{\beta}_{\lambda\alpha,\lambda'\alpha'} = (E_\lambda + E_\alpha)\delta_{\lambda\lambda'}\delta_{\alpha\alpha'} + \mathscr{V}^{\beta}_{\lambda\alpha,\lambda'\alpha'}. \tag{4.14}$$

The phonon-phonon potential is given by

$$\mathscr{V}^{\beta}_{\lambda\alpha,\lambda'\alpha'} = \sum_{\sigma} W(\beta\lambda'\alpha\sigma;\alpha'\lambda)\mathscr{F}_{\lambda\alpha,\lambda'\alpha'}, \tag{4.15}$$

where

$$\mathscr{F}_{\lambda\alpha,\lambda'\alpha'} = \sum_{rstq} F^{\sigma}_{rsqt}\rho_{\alpha\alpha'}([r\times s]^{\sigma})\rho_{\lambda\lambda'}([q\times t]^{\sigma}). \tag{4.16}$$

One may notice the formal analogy of the structure of the phonon matrix $\mathscr{A}_{\lambda\alpha,\lambda'\alpha'}$ with the form (2.15) of the TDA matrix $A_{ph,p'h'}$. Formally the first is deduced by the second by replacing the the p-h energies with the sum of phonon energies and the p-h interaction with a phonon-phonon potential . This corrispondence can be illustrated in terms of diagrams. The TDA p-h lines are replaced by phonons (Fig. 4.1) and each TDA p-h vertex is turned into a phonon phonon vertex (Fig. 4.2) which amounts to a sum of infinite diagrams in the two-body potential.

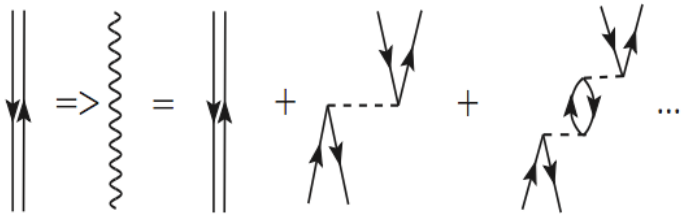

Figure 4.1: From p-h to phonons

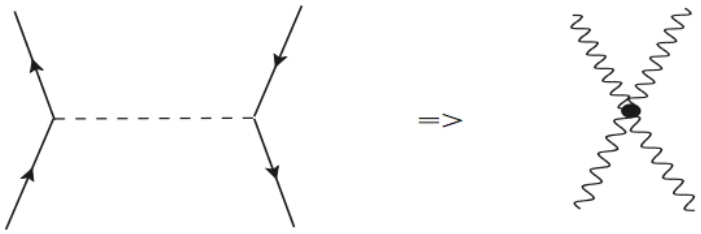

Figure 4.2: From p-h vertices to phonon-phonon vertices

Unlike the TDA, however, the Eq. (4.13) is not yet an eigenvalue equation. This is obtained expressing the amplitudes $X^{\beta}_{\lambda\alpha}$ in terms of the expansion coefficients $C^{\beta}_{\lambda\alpha}$ of the basic using the relation (4.8). We get

$$\sum_{\lambda'\alpha'} H^{\beta}_{\lambda\alpha\lambda'\alpha'} C^{\beta}_{\lambda'\alpha'} = \sum_{\lambda'\alpha'} (A\mathscr{D})^{\beta}_{\lambda\alpha\lambda'\alpha'} C^{\beta}_{\lambda'\alpha'} = E_{\beta} \sum_{\lambda'\alpha'} \mathscr{D}_{\lambda\alpha,\lambda'\alpha'} C^{\beta}_{\lambda'\alpha'}, \qquad (4.17)$$

which in short becomes

$$HC = (A\mathscr{D})C = EDC. \qquad (4.18)$$

This represents a generalized eigenvalue problem in the overcomplete basis $|(\lambda \times \alpha)^{\beta}\rangle$. By resorting to a procedure based on Cholesky decomposition (App. B), that select a basis of linearly independent states spanning the physical subspace of the correct dimension $(N_n < N_r)$, we construct a non singular overlap matrix D_n, and by left multiplication in the N_n-dimensional subspace we get from Eq. (4.18)

$$[D_n^{-1}(A\mathscr{D})_n]C = EC. \qquad (4.19)$$

This equation determines only the coefficient $C^{\beta}_{\lambda\alpha}$ of the N_n-dimensional physical subspace. The remaining $N_r - N_n$ redundant coefficients are undetermined and, therefore, can be put safely equal to zero.

Since recursive formulas hold for all quantities entering A and D, it is possible to solve the eigenvalue equations iteratively starting from the TDA phonons and, thereby, generate a basis of orthonormal multiphonon states $\{|\,0\rangle \mid \alpha_1\rangle(=|\,\lambda\rangle), |\,\alpha_2\rangle \ldots\ldots \mid \alpha_n\rangle\}$. Such a basis can be adopted to diagonalize the Hamiltonian in a multiphonon space.

4.1.2 Eigenvalue problem in the multiphonon basis

The Hamiltonian in the multiphonon basis is diagonal within each n-phonon subspace and can be written as

$$\sum_{n'\beta_{n'}} \left[(E_{\alpha_n} - E_\nu)\, \delta_{nn'} \delta_{\alpha_n \beta_{n'}} + \mathscr{V}_{\alpha_n \beta_{n'}} \right] \mathrm{C}^{\nu}_{\beta_{n'}} = 0, \tag{4.20}$$

where the only nonvanishing terms of the potential are those connecting states differing by one or two phonons

$$\mathscr{V}_{\alpha_n \beta_{n'}} = \langle \alpha_{n-1} | H | \beta_n \rangle + < \alpha_{n-2} | H | \beta_n > . \tag{4.21}$$

The first term is given by

$$\langle \alpha_{n-1} | H | \beta_n \rangle = \sum_{\sigma \alpha'} \mathscr{V}^{\alpha}_{\sigma \alpha'} X^{\beta}_{\alpha' \sigma}(n), \tag{4.22}$$

whith

$$\mathscr{V}^{\alpha}_{\sigma \alpha'} = [\beta]^{-1} (-)^{\beta + \alpha' + \sigma} \sum_{rsph} c^{\sigma}_{ph} F^{\sigma}_{phrs} \rho_{\alpha \alpha'}([r \times s]^{\sigma}). \tag{4.23}$$

The second term is

$$\langle \alpha_{n-2} \mid H \mid \beta_n \rangle = [\beta]^{-1} \sum_{\sigma \sigma' \gamma} (-)^{\beta + \gamma + \sigma} \delta_{J_\sigma J_{\sigma'}} X^{\beta}_{\gamma \sigma}(n) X^{\gamma}_{\alpha \sigma'}(n-1) \mathscr{V}_{\sigma \sigma'}, \tag{4.24}$$

where

$$\mathscr{V}_{\sigma\sigma'} = \frac{1}{4}\delta_{J_\sigma J_{\sigma'}} \sum_{php_1h_1} F^{\sigma}_{php_1h_1} c^{\sigma}_{ph} c^{\sigma'}_{p_1h_1}. \tag{4.25}$$

Special cases of the above coupling terms are illustrated in Fig. (4.3).

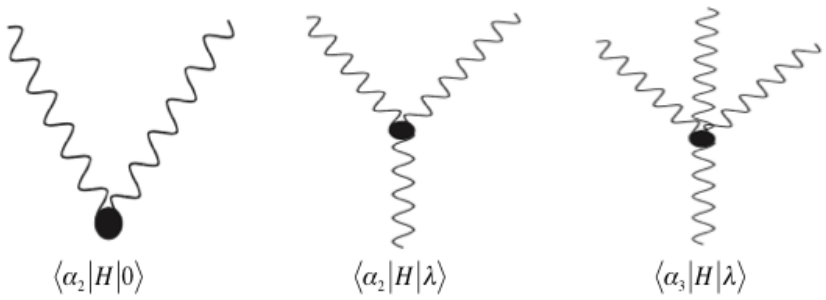

Figure 4.3: phonon-phonon vertices

The solution yields to the final eigenvalues E^ν and the corresponding eigenfunctions

$$|\Psi_\nu\rangle = \sum_{\alpha_n} \mathrm{C}^\nu_{\alpha_n} |\alpha_n\rangle. \tag{4.26}$$

The above formula holds also for the ground state which, therefore, is explicitly correlated. In fact, as shown in Fig. (4.4), the vertex coupling the $n = 0$ to the $n = 2$ phonon states amounts to a sum of an infinite series of diagrams promoting a highly correlated ground state. Indeed, our multiphonon eigenvalue problem is equivalent to shell model and extends RPA without having to rely on any approximation.

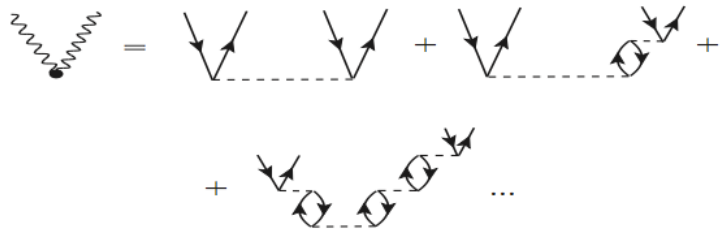

Figure 4.4: Ground state correlation in the lowest order of phonon-phonon interaction

4.1.3 Transition Amplitudes

The eigenstates obtained (4.26) may be used to compute the transition amplitudes. For a one-body multipole operator of the form (2.18) we have

$$\begin{aligned}
&\langle \Psi_f \parallel \mathscr{M}(\lambda) \parallel \Psi_i \rangle = \sum_{nn'\alpha_n\beta_{n'}} \mathrm{C}^i_{\alpha_n} \mathrm{C}^f_{\beta_{n'}} \langle \beta_{n'} \parallel \mathscr{M}(\lambda) \parallel \alpha_n \rangle \\
&= \sum_{n\alpha_n\beta_{n+1}} \mathrm{C}^i_{\alpha_n} \mathrm{C}^f_{\beta_{n+1}} \langle \beta_{n+1} \parallel \mathscr{M}(\lambda) \parallel \alpha_n \rangle + \\
&+ \sum_{n\alpha_n\beta_{n-1}} \mathrm{C}^i_{\alpha_n} \mathrm{C}^f_{\beta_{n-1}} \langle \beta_{n-1} \parallel \mathscr{M}(\lambda) \parallel \alpha_n \rangle + \\
&+ \sum_{n\alpha_n\beta_n} \mathrm{C}^i_{\alpha_n} \mathrm{C}^f_{\beta_n} \langle \beta_n \parallel \mathscr{M}(\lambda) \parallel \alpha_n \rangle, \qquad (4.27)
\end{aligned}$$

where

$$\langle \beta_{n+1} \parallel \mathscr{M}(\lambda) \parallel \alpha_n \rangle = (-)^{J_\beta - J_\alpha - \lambda} \frac{1}{[\lambda]^{1/2}} \sum_{x_\lambda} X^{\beta}_{(x_\lambda \lambda)\alpha} \mathscr{M}_\lambda [0 \to (x_\lambda \lambda)], \qquad (4.28)$$

$$\langle \beta_{n-1} \parallel \mathscr{M}(\lambda) \parallel \alpha_n \rangle = (-)^{\lambda} \frac{1}{[\lambda]^{1/2}} \sum_{x_\lambda} X^{\alpha}_{(x\lambda)\beta} \mathscr{M}_\lambda [0 \to (x_\lambda \lambda)], \qquad (4.29)$$

$$\langle \beta_n \parallel \mathscr{M}(\lambda) \parallel \alpha_n \rangle = \sum_{rs} \langle r \parallel \mathscr{M}_\lambda \parallel s \rangle \langle \beta_n, \parallel (a^\dagger_r \times b_s)^\lambda \parallel \alpha_n, \rangle. \qquad (4.30)$$

The terms $\mathscr{M}[0 \to (x_\lambda \lambda)]$ are the TDA transition amplitudes (2.19)

$$\mathscr{M}_\lambda[0 \to (x_\lambda \lambda)] = \langle x_\lambda \lambda \parallel \mathscr{M}(\lambda) \parallel 0 \rangle. \tag{4.31}$$

The matrix elements (4.28) and (4.29) couple states differing by one phonon, the other term (4.30) describes a scattering transition between states with the same number of phonons.

4.2 The EMPM in the quasiparticle scheme

In the qp basis we start from the HFB vacuum and use the QTDA phonons to generate an orthonormal multiphonon basis for solving the eigenvalue problem.

4.2.1 Generation of the multiphonon basis

In the qp scheme the basis to be derived is of the form

$$\mid \beta_n\rangle = \sum_{\lambda\,\alpha_{n-1}} \mathrm{C}^{\beta_n}_{\lambda\,\alpha_{n-1}} \left\{ O^\dagger_\lambda \times \mid \alpha_{n-1} \right\}^\beta, \tag{4.32}$$

where $O^\dagger_\lambda$ is the QTDA phonon operator given by

$$O^\dagger_\lambda = \sum_{rs} \zeta_{rs} C^\lambda_{rs} \left(\alpha^\dagger_r \times \alpha^\dagger_s \right). \tag{4.33}$$

Following the same procedure outlined for the p-h case, we start with constructing the equations of motion in the n-phonon subspace

$$\langle \beta \parallel [H, O^\dagger_\lambda] \parallel \alpha \rangle = \Big(E_\beta - E_\alpha \Big) X^\beta_{\lambda\alpha}, \tag{4.34}$$

where

$$X^\beta_{\lambda\alpha} = \langle \beta \parallel O^\dagger_\lambda \parallel \alpha \rangle = \sum_{\lambda'\alpha'} \mathscr{D}^\beta(\lambda\alpha, \lambda'\alpha') C^\beta_{\lambda'\alpha'}. \tag{4.35}$$

Here $\mathscr{D}^\beta(\alpha\lambda;\alpha'\lambda')$ is the metric or overlap matrix. We have omitted the subscript n for simplicity.

After expanding the commutator and making use of the relation (4.35) we obtain the generalized eigenvalue equations

$$\sum_{\lambda_1\alpha_1\lambda'\alpha'} \Big[\mathscr{A}^\beta(\lambda\alpha, \lambda'\alpha') - E_\beta \delta_{\lambda\lambda'}\delta_{\alpha\alpha'} \Big] \mathscr{D}^\beta(\lambda'\alpha', \lambda_1\alpha_1) C^\beta_{\lambda_1\alpha_1} = 0, \tag{4.36}$$

where $\mathscr{A}$ is a matrix of the simple structure

$$\mathscr{A}^{\beta}(\lambda\alpha,\lambda'\gamma) = (E_{\lambda}+E_{\alpha})\delta_{\lambda\lambda'}\delta_{\alpha\gamma}+\mathscr{V}^{\beta}_{\lambda\alpha,\lambda'\gamma}. \tag{4.37}$$

The phonon-phonon potential $\mathscr{V}^{\beta}$ is given by

$$\mathscr{V}^{\beta}_{\lambda\alpha,\lambda'\gamma} = \sum_{\sigma} W(\beta\lambda'\alpha\sigma;\gamma\lambda)\mathscr{V}^{\sigma}_{\lambda\alpha,\lambda'\gamma}, \tag{4.38}$$

where

$$\mathscr{V}^{\sigma}_{\lambda\alpha,\lambda'\gamma} = \frac{1}{2}\sum_{rtsq} V^{\sigma}_{rtsq}(22)\rho_{\lambda\lambda'}([r\times t]^{\sigma})\rho_{\alpha\alpha'}([s\times q]^{\sigma}). \tag{4.39}$$

Here the term $\mathscr{V}^{\sigma}_{rtsq}(22)$ has been defined in the Eq. (3.9), and $\rho_{\lambda\lambda'}([r\times t]^{\sigma})$ is the n-phonon density matrix.

The Eq. (4.36) represents a generalized egenvalue problem in the overcomplete basis $\left\{O^{\dagger}_{\lambda}\times \mid \alpha_{n-1}>\right\}^{\beta}$. We turn this singular equation into a regular one by using the same procedure outlined in the p-h scheme, based on the Cholesky decomposition method (App. B).

The eigenvalue problem within the n-phonon subspace is thereby solved exactly and yields a basis of orthonormal correlated n-phonon states of the form given by the Eq. (4.32).

4.2.2 Eigenvalue problem in the multiphonon basis

We can use this multiphonon basis to diagonalize the hamiltonian that takes the form

$$\sum_{n'\beta_{n'}}\left[\left(E_{\alpha_n}-E^{\nu}\right)\delta_{nn'}\delta_{\alpha_n\beta_{n'}}+\mathscr{V}_{\alpha_n\beta_{n'}}\right]\mathrm{C}^{\nu}_{\alpha'} = 0, \tag{4.40}$$

where the potential has the structure

$$\mathscr{V}_{\alpha_n\beta_{n'}} = \delta_{n'(n-1)}\mathscr{V}^{(31)}_{\alpha_n\beta_{n'}}+\delta_{n'(n-2)}\mathscr{V}^{(40)}_{\alpha_n\beta_{n'}}. \tag{4.41}$$

The matrix elements of $\mathcal{V}^{(31)}$ are

$$\mathcal{V}^{(31)}_{\alpha\beta} = [\alpha]^{-1} \sum_{\sigma\gamma} (-)^{\alpha+\gamma+\sigma} \mathcal{V}^{\sigma}_{\beta\gamma} X^{(\alpha)}_{\sigma\gamma}, \tag{4.42}$$

where

$$\mathcal{V}^{\sigma}_{\beta\gamma} = \sum_{tq} \mathcal{V}^{\sigma}_{tq} \rho^{(n')}_{\beta\gamma}([t \times q]^{\sigma}), \tag{4.43}$$

and

$$\mathcal{V}^{\sigma}_{tq} = \frac{1}{2} \sum_{r \le s} c^{\sigma}_{rs} \zeta_{rs} \Big[F^{\sigma}_{rstq} (u_r v_s u_t u_q - v_r u_s v_t v_q) + \\ + (-)^{t-q-\sigma} F^{\sigma}_{rsqt} (u_s v_r u_t u_q - v_s u_r v_t v_q) \Big]. \tag{4.44}$$

For $\mathcal{V}^{(40)}_{\alpha\beta}$ we have

$$\mathcal{V}^{(40)}_{\alpha\beta} = [\alpha]^{-1} \sum_{xy\sigma\gamma} (-)^{\alpha+\gamma+\sigma} X^{\alpha}_{(x\sigma)\gamma} X^{\gamma}_{(y\sigma)\beta} \mathcal{V}^{(\sigma)}_{xy}, \tag{4.45}$$

where

$$\mathcal{V}^{(\sigma)}_{xy} = \frac{1}{4} \sum_{(r \le s)(t \le q)} \zeta_{rs} \zeta_{tq} c^{\sigma}_{rs}(x) c^{\sigma}_{tq}(y) \times \Big[F^{\sigma}_{rstq} (u_r v_s u_t v_q + u_s v_r u_q v_t) \\ + (-)^{r-s-\sigma} F^{\sigma}_{srtq} (u_s v_r u_t v_q + u_r v_s u_q v_t) \Big]. \tag{4.46}$$

The solution of the full eigenvalue equations (4.40) yields the final eigenvalues E_ν and the corresponding eigenfunctions

$$\mid \Psi_\nu \rangle = \sum_{\alpha_n} \mathrm{C}^{\nu}_{\alpha_n} \mid \alpha_n \rangle, \tag{4.47}$$

where $\mid \alpha_n \rangle$ form a basis of orthonormal n-phonon states of the structure given by (4.32).

4.2.3 Transition amplitudes

The eigenfunctions so obtained may be used to compute the transition amplitudes. For a one-body λ-multipole operator of the form (2.18) we have

$$\langle \Psi_f \parallel \mathscr{M}(\lambda) \parallel \Psi_i \rangle = \sum_{n\alpha_n\beta_{n+1}} \Big[\mathrm{C}^f_{\beta_{n+1}} \mathrm{C}^i_{\alpha_n} \langle \beta_{n+1} \parallel \mathscr{M}(\lambda) \parallel \alpha_n \rangle + (-)^{J_\beta - J_\alpha} \mathrm{C}^f_{\beta_{n-1}} \mathrm{C}^i_{\alpha_n} \langle \alpha_n \parallel \mathscr{M}(\lambda) \parallel \beta_{n-1} \rangle + \mathrm{C}^f_{\beta_n} \mathrm{C}^i_{\alpha_n} \langle \beta_n \parallel \mathscr{M}(\lambda) \parallel \alpha_n \rangle \Big], \tag{4.48}$$

where

$$\langle \beta_{n+1} \parallel \mathscr{M}(\lambda) \parallel \alpha_n \rangle = [\lambda]^{-1/2} \sum_{x_\lambda} \mathscr{M}[0 \to (x_\lambda \lambda)] X^{\beta}_{(x_\lambda \lambda)\alpha}, \tag{4.49}$$

$$\langle \alpha_n \parallel \mathscr{M}(\lambda) \parallel \beta_{n-1} \rangle = [\lambda]^{-1/2} \sum_{x_\lambda} \mathscr{M}[0 \to (x_\lambda \lambda)] X^{\alpha}_{(x_\lambda \lambda)\beta}, \tag{4.50}$$

$$\langle \beta_n \parallel \mathscr{M}(\lambda) \parallel \alpha_n \rangle = [\lambda]^{-1/2} \sum_{rs} \mathscr{M}^{(-)}_{rs}(\lambda) \rho_{\alpha_i \beta_f}([r \times s]^\lambda). \tag{4.51}$$

Here $\mathscr{M}[0 \to (x_\lambda \lambda)]$ are the QTDA transition amplitudes (3.23)

$$\mathscr{M}[0 \to (x_\lambda \lambda)] = \langle x_\lambda \lambda \parallel \mathscr{M}(\lambda) \parallel 0 \rangle, \tag{4.52}$$

and $\mathscr{M}^{(-)}_{rs}(\lambda)$ are the scattering transitions given by

$$\mathscr{M}^{(-)}_{rs}(\lambda) = \langle r \parallel \mathscr{M}_\lambda \parallel s \rangle \Big(u_r v_s - (-)^\lambda u_s v_r \Big). \tag{4.53}$$

The matrix elements (4.49) and (4.50) couple states differing by one phonon, the other term (4.51) describes a scattering transition between states with the same number of phonons.

4.3 The EMPM for odd-even nuclei

Different methods have been developed to study the modifications of the single-particle states in odd nuclei induced by the core excitations. The basic mechanism is illustrated within the particle-vibration coupling (PVC) model [1, 49] in which a particle is coupled to the collective excitations of the core, commonly described in random-phase approximation (RPA). Recently, PVC calculations were performed within the framework of energy density functionals deduced from Skyrme forces [50, 51, 52] or relativistic meson-nucleon Lagrangians [41, 53] or from the theory of finite Fermi systems [54].

Calculations using NN + 3N chiral forces were performed within the context of self-consistent Green's function theory [55], no-core shell model (NCSM) [56] and coupled cluster [57, 58, 59].

The corrections induced by the core excitations to the single-particle energies have been studied also within the EMPM [60, 61]. In its extension to odd nuclei an analogous set of equations is derived and solved iteratively to generate an orthonormal basis of states composed of a valence particle coupled to n-phonon states $(n = 1,2,...n...)$, also generated within the EMPM, describing the excitations of a doubly magic core. The basis is then adopted to solve the full eigenvalue problem.

4.3.1 Generation of the multiphonon basis

We intend to generate an orthonormal basis of the form

$$|\nu_n\rangle = \sum_{p\alpha_n} C^{\nu_n}_{p\alpha_n} |(p \times \alpha_n)^\nu\rangle = \sum_{p\alpha_n} C^{\nu_n}_{p\alpha_n} \left\{ a^\dagger_p \times |\alpha_n\rangle \right\}^\nu , \tag{4.54}$$

where $\mid \alpha_n\rangle$ are the n-phonon core states (4.1) also derived within the EMPM. In the following derivation we will omit the subscript n when we are confined within a n-phonon subspace. In close analogy with the previous cases we start with the equations of motion

$$\langle \alpha \parallel [b_p, H]^p \parallel \nu \rangle = (E_\nu - E_\alpha) X^\nu_{p\alpha}, \tag{4.55}$$

where

$$X^\nu_{p\alpha} = \langle \alpha \parallel b_p \parallel \nu \rangle = \sum_{p'\alpha'} \mathscr{D}^\nu(p\alpha, p'\alpha') C^\nu_{p'\alpha'}. \tag{4.56}$$

The quantities $X^\nu_{p\alpha}$ and $C^\nu_{p'\alpha'}$ satisfy the normalization condition

$$1 = \langle \nu \mid \nu \rangle = [\nu]^{-1/2} \sum_{p\alpha} X^\nu_{p\alpha} C^\nu_{p\alpha}. \tag{4.57}$$

The matrix $\mathscr{D}(p\alpha, p'\alpha')$ is the metric of the basis $|(p \times \alpha_n)^\nu\rangle$ defined by

$$\begin{aligned} \mathscr{D}^\nu(p'\lambda', p\lambda) &= \langle \overline{(p' \times \lambda')^\nu} \mid (p \times \lambda)^\nu \rangle = \delta_{pp'} \delta_{\lambda\lambda'} \\ -\sum_\sigma [\sigma]^{1/2} (-)^{p-\nu+\lambda} W(p'p\lambda'\lambda; \sigma\nu) &\langle \lambda' \parallel (a^\dagger_p \times b_{p'})^\sigma \parallel \lambda \rangle. \end{aligned} \tag{4.58}$$

It reintroduces, through the density matrix ρ (4.10), the exchange terms among the odd particle and the n-phonon states, thereby re-establishing the Pauli principle.

After expanding the commutator in the left-hand member of the Eq. (4.55) we obtain

$$\sum_{p'\alpha' p_1 \alpha_1} \left\{ (\varepsilon_p + E_\alpha - E_\nu) \delta_{pp'} \delta_{\alpha\alpha'} + \mathscr{V}_{p\alpha p'\alpha'} \right\} \mathscr{D}^\nu(p'\alpha', p_1\alpha_1) C^\nu_{p_1\alpha_1} = 0. \tag{4.59}$$

The interaction part is given by

$$\mathscr{V}_{p\alpha p'\alpha'} = \sum_\sigma [\sigma]^{1/2} W(\alpha\sigma\nu p'; \alpha' p) \mathscr{F}_{p\alpha p'\alpha'} \tag{4.60}$$

where

$$\mathscr{F}_{p\alpha p'\alpha'} = \sum_{\sigma tq} F^{\sigma}_{pp'tq}\rho_{\alpha\alpha'}([t\times q]^{\sigma}). \tag{4.61}$$

The equation (4.59) is singular since the basis (4.54) is overcomplete. Following the same procedure adopted for the even-even case based on Cholesky decomposition (App. B), we extract a basis of linearly independent states and obtain a non singular eigenvalue problem. Its iterative solutions give the particle-core states $\{|\,\nu_1\rangle ... |\,\nu_n\rangle\}$, which, together with the single particle states $|\,\nu_0\rangle$, form an orthonormal basis.

4.3.2 Eigenvalue problem in the multiphonon basis

Once we have generated, iteratively, the multiphonon basis, we can solve the eigenvalue problem in such a basis

$$\sum_{\nu_{n'}} \left[(E_{\nu_n} - E^{\nu})\,\delta_{\nu_n\nu_{n'}} + \mathscr{V}_{\nu_n\nu_{n'}} \right] C^{\nu}_{\nu_{n'}} = 0, \tag{4.62}$$

where the interaction part has non vanishing matrix elements for $n' = n\pm 1, n\pm 2$, and is given by

$$\mathscr{V}_{\nu_n\nu_{n'}} = [v]^{-1/2} \sum_{p\alpha_n, p'\alpha_{n'}} C^{\nu_n}_{p\alpha_n}\, \mathscr{V}^{\nu}_{p\alpha_n, p'\alpha_{n'}} X^{\nu_{n'}}_{p'\alpha_{n'}}. \tag{4.63}$$

The potential $\mathscr{V}^{\nu}_{p\alpha_n, p'\alpha_{n'}}$ is defined by

$$\mathscr{V}^{\nu}_{p\alpha_n, p'\alpha_{n'}} = \delta_{pp'}\langle\alpha_n|H|\alpha_{n'}\rangle + \delta_{n'(n+1)} \sum_{\lambda} W(\alpha_{n'}\lambda\nu p; \alpha_n p')\, X^{\alpha_{n'}}_{\lambda\alpha_n}\, \mathscr{F}^{\lambda}_{pp'}, \tag{4.64}$$

where

$$\mathscr{F}^{\lambda}_{pp'} = \sum_{p_1 h_1} F^{\lambda}_{pp'p_1h_1} c^{\lambda}_{p_1h_1}. \tag{4.65}$$

The eigenvalue equation (4.62) yields all the eigenvalues allowed by the space dimensions, and the eigenfunctions have the structure

$$\Psi_\nu = \sum_{\nu_n} C^\nu_{\nu_n} |\nu_n\rangle. \tag{4.66}$$

4.3.3 Transition amplitudes

Starting from the multipole operator in coupled scheme (2.18) the transition amplitudes in the multiphonon particle-core basis take the form

$$\langle \nu_{n'} \parallel \mathscr{M}(\lambda) \parallel \nu_n \rangle = \sum_{nn'} \mathscr{M}^{(\nu\nu')}_{nn'}(\lambda), \tag{4.67}$$

where

$$\mathscr{M}^{(\nu\nu')}_{nn'}(\lambda) = \frac{1}{[\lambda]^{1/2}} \sum_{rs} \langle r \parallel \mathscr{M}_\lambda \parallel s \rangle \langle \nu_{n'} \parallel (a^\dagger_r \times b_s)^\lambda \parallel \nu_n \rangle. \tag{4.68}$$

If the initial/final states have dominant particle character we can truncate the above formula and get

$$\langle \nu_{n'} \parallel \mathscr{M}(\lambda) \parallel \nu_n \rangle = \mathscr{M}^{(\nu\nu')}_{00} + \mathscr{M}^{(\nu\nu')}_{10} + \mathscr{M}^{(\nu\nu')}_{01}, \tag{4.69}$$

where $\mathscr{M}^{(\nu\nu')}_{00}$, $\mathscr{M}^{(\nu\nu')}_{10}$ and $\mathscr{M}^{(\nu\nu')}_{01}$ are respectively the particle-particle, particle-phonon and phonon-particle transition amplitudes, given by

$$\mathscr{M}^{(\nu\nu')}_{00}(\lambda) = \sum_{pp'} C^\nu_p C^{\nu'}_{p'} \langle p' \parallel \mathscr{M}_\lambda \parallel p \rangle, \tag{4.70}$$

$$\mathscr{M}^{(\nu\nu')}_{01}(\lambda) = \sum_p C^\nu_p \sum_{x_\lambda} \mathscr{M}(0 \to [x_\lambda \lambda]) \sum_{\nu'_1} C^{\nu'}_{\nu'_1} X^{\nu'_1}_{p\lambda}, \tag{4.71}$$

$$\mathscr{M}^{(\nu\nu)}_{10}(\lambda) = \sum_{p'} (-)^{\nu'-\nu} C^{\nu'}_{p'} \sum_{x_\lambda} \mathscr{M}(0 \to [x_\lambda \lambda]) \sum_{\nu_1} C^\nu_{\nu_1} X^{\nu_1}_{p'\lambda}, \tag{4.72}$$

where

$$\mathscr{M}(0 \to [x_\lambda \lambda]) = [\lambda]^{-1/2} \sum_{ph} \langle p \parallel \mathscr{M}_\lambda \parallel h \rangle c_{ph}^{(x_\lambda \lambda)}. \tag{4.73}$$

are the amplitudes of the transitions to the x_{th} TDA state with $J_x = \lambda$.

Chapter 5

Application of the EMPM to even-even nuclei

5.1 Choice of the Hamiltonian

We use the intrinsic Hamiltonian

$$H = T_{int} + V_2 = T + V_2 + T_2, \tag{5.1}$$

where

$$T_{int} = \frac{1}{2m}\sum_i p_i^2 - T_{CM}, \tag{5.2}$$

is the intrinsic kinetic operator and V_2 is the chiral two body potential $NNLO_{opt}$ [62] derived by fixing the coupling constants at next-to-next leading order through a new optimization method in the analysis of the phase shifts, which minimizes the effects of the three-nucleon force. This potential, however, produces too much attraction in medium and heavy mass nuclei and overestimates their binding energies.

The full Hamiltonian can be written in the standard form

$$H = T + V, \tag{5.3}$$

where

$$T = \left(1 - \frac{1}{A}\right) \frac{1}{2m} \sum_i p_i^2, \tag{5.4}$$

is a modified one-body kinetic term and

$$V = V_2 + T_2, \tag{5.5}$$

includes the two-body kinetic term

$$T_2 = \frac{1}{2mA} \sum_{i \neq j} \vec{p}_i \cdot \vec{p}_j. \tag{5.6}$$

5.2 $E1$ response in nuclei

Our calculations will focus mainly on the study of the giant dipole resonance (GDR) and the pygmy dipole resonance (PDR).

The GDR is the most famous and studied nuclear resonance observed in all nuclei. It appears as a large hump of width $\sim 5MeV$ around a main peak. Its centroid lies at an energy

$$E_{1^-}^{GR} \sim 79A^{-1/3}. \tag{5.7}$$

The first theoretical interpretation of the GDR was given, within the classical context, by Goldhaber and Teller in 1948 [63]. They interpreted this resonance as arising from a rigid translations of protons versus neutrons (Fig. 5.1 (b)). This model yields a level of energy $E \sim A^{-1/6}$.

Steinwedel e Jensen in 1950 gave a more accurate description [64] within an hydrodynamic model. The resonance originates from a local oscillation of

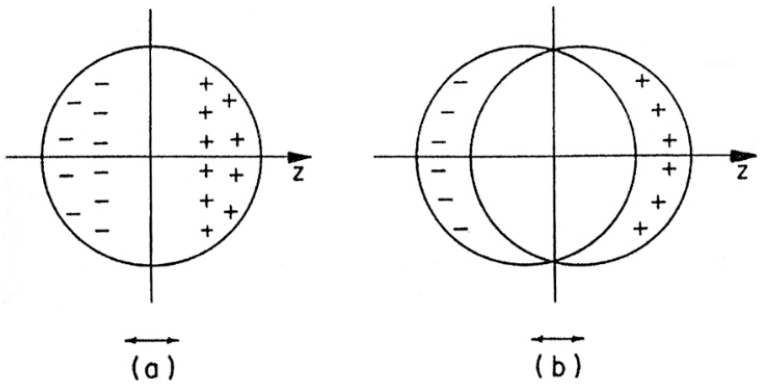

Figure 5.1: Schematic representation of nuclear dipole oscillation, within Steinwedel and Jensen model (a), and Goldhaber-Teller model (b).

neutrons and protons confined within an incompressible fluid (Fig. 5.1 (a)). This model predicts $E \sim A^{-1/3}$ consistently with the experimental observations.

The PDR is a resonance located along the queue of the GDR. Its first experimental evidence was provide by a systematic study of γ-rays after thermal neutron capture [65].

The interest toward such a mode has increased dramatically with the advent of radioactive beams. These new techniques have produced a large amount of data which made possible a more reliable investigation of the neutron skin thickness and of the symmetry energy. Moreover has been provided informations relevant to neutron stars and other astrophysical phenomena [66, 67, 68]

Several different techniques were employed successfully in the search of low-lying dipole transitions in stable and unstable neutron rich nuclei. Radioactive beam experiments have extracted an appreciable dipole strength just above the neutron decay threshold in unstable nuclei, like neutron rich oxygen [69] or tin

isotopes around ^{132}Sn [70]. More detailed data were obtained for stable nuclei by combining (γ,γ') [71, 72, 73, 74] with $(\alpha,\alpha'\gamma)$ measurements [75, 76, 77, 78, 79], or via inelastic scattering of ^{17}O ions [80, 81, 82].

The first theoretical interpretation of the PDR was given by Mohan at al. [83] in a three fluids dynamical model. Within this model two independent $E1$ resonances occur, one originated from the oscillation of the proton against the neutron, another, lower in energy, from the oscillation of the neutron excess against an $N = Z$ core.

Many calculations were carried out in HF plus RPA [84, 85, 86, 87] or, for open shell nuclei, within HFB plus QRPA [88, 89, 90, 91]. Recently some calculations have investigated the relevance of the mode to the neutron skin and the symmetry energy [92, 93, 94].

The fragmentation of the GDR and the fine structure of the pygmy were studied by several approaches, like QRPA plus phonon coupling [95], second RPA [11] the quasiparticle-phonon model (QPM) [36], and the relativistic quasiparticle time-blocking approximation (RTBA) [96].

We have adopted our EMPM to investigate the dipole response in the heavy, neutron-rich, ^{132}Sn [46] and ^{208}Pb [47]. Recently the method has been adopted in the qp scheme to study the spectra and the dipole respone in the neutron rich oxygen isotope ^{20}O [48].

5.3 Investigation of the $E1$ response in ^{132}Sn and ^{208}Pb within the EMPM

We have used the intrinsic Hamiltonian (5.3) to compute the HF basis in a configuration space which includes all the harmonic oscillator major shells up to $N_{max} = 12$.

As shown in Fig. (5.2 (i)), the HF levels generated by the $NNLO_{opt}$ are too far apart with respect to the experimental ones. This is common to all HF spectra derived from other NN interactions [26, 97].

In order to get a more compressed single particle spectra we added a phenomenological repulsive density-dependent term V_ρ

$$V_\rho = \frac{C_\rho}{6}(1+P_\sigma)\rho\left(\frac{(\vec{r}_1+\vec{r}_2)}{2}\right)\delta(\vec{r}_1-\vec{r}_2). \tag{5.8}$$

This term was deduced from a three-body contact term [98]

$$V_3 = C_\rho\delta(\vec{r}_1-\vec{r}_2)\delta(\vec{r}_2-\vec{r}_3), \tag{5.9}$$

and contain a free parameter C_ρ.

As shown in Ref. [99] it improved the description of bulk properties in closed shell nuclei within a HF plus perturbation theory approach.

The TDA phonons are generated using a restricted number of major shells. We have used three major shells above and three below the Fermi surface. We obtain however basically the same results if the calculations were carried out in a more restricted space using three major shells above and one below the Fermi surface.

As shown in Fig. (5.2) for ^{132}Sn, the added density-dependent term produces a strong compression of the single particle levels. The spectrum however deviates from the empirical one in several important details [100]. The levels within a

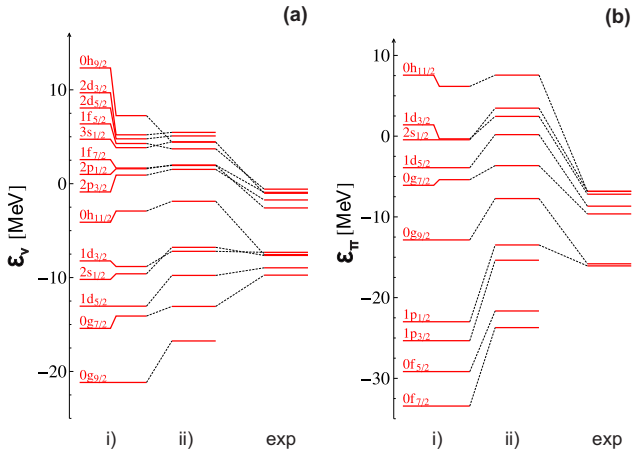

Figure 5.2: Neutron (a) and proton (b) single particle spectra in ^{132}Sn with (i) $V = V_2$ and (ii) $V = V_2 + V_\rho$. The empirical (exp) single-particle levels are taken from [100].

major shell are not sufficiently packed while the spin-orbit intruders are not sufficiently pushed down.

The free parameter was fixed so as to reproduce roughly the main peak of the GDR (Fig. 5.3). We obtain $C_\rho \sim 1000$ MeV fm^6 in ^{132}Sn, and $C_\rho \sim 2000$ MeV fm^6 in ^{208}Pb.

5.3.1 EMPM results

The EMPM calculations were carried out in a space which encompassed up to a truncated set of two-phonon basis states. We include the states $|\,(\lambda_1 \times \lambda_2)^\beta\rangle \equiv \{O^\dagger_{\lambda_1} \times |\,\lambda_2\rangle\}^\beta$ with $(E_{\lambda_1} + E_{\lambda_2}) \leq 30$ MeV for ^{132}Sn. In the case of ^{208}Pb, we include all the TDA phonon states with dominant $1\hbar\omega$ component and all the two phonon states with $(E_{\lambda_1} + E_{\lambda_2}) \leq 20$ MeV and $E_{\lambda_1} \leq 15$ MeV.

The ground state of ^{132}Sn and ^{208}Pb get depressed with respect to their un-

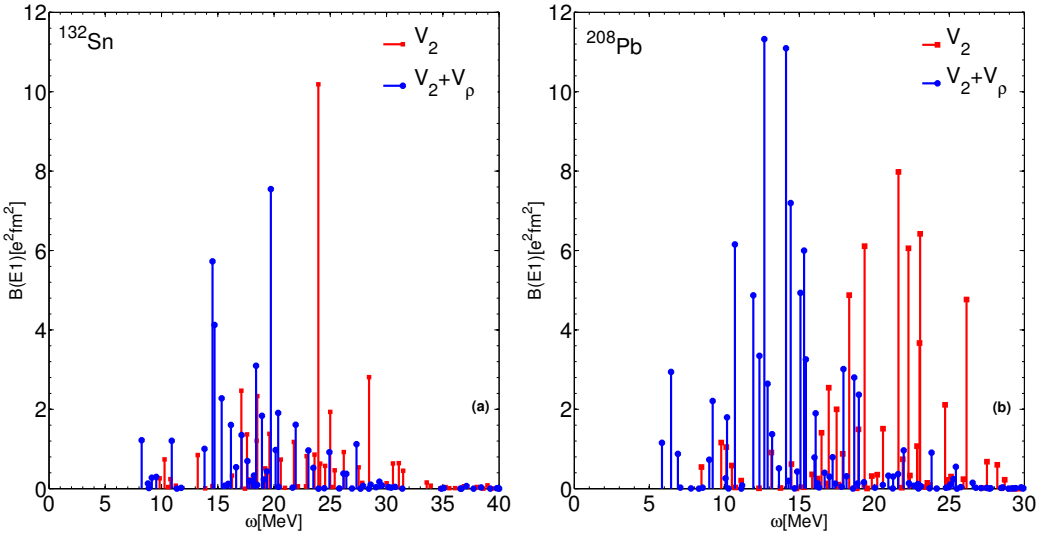

Figure 5.3: TDA $E1$ spectra with $V_2 = NNLO_{opt}$ only and $V_2 = NNLO_{opt} + V_\rho$ in ^{132}Sn (a) and ^{208}Pb (b).

perturbed HF states by $\Delta E = 10.5$ MeV and $\Delta E = 7.3$ MeV respectively. Their two phonon components account for 23% and 24% of their total wave functions. These large shift would spoil the description of the dipole response by pushing the excited states, and therefore the strength, at too high energy.

The corrected separation between the ground and the excited states would be restored with the inclusion of the three phonon states as shown for ^{16}O in Ref. [20]. Including three phonons however is not an easy task since the dimension of the space would become too large. We, therefore, refer the excited levels to the HF vacuum rather then the correlated ground state consistently with shell model calculation [101].

In order to study the properties of the $E1$ response we compute the $E1$ reduced

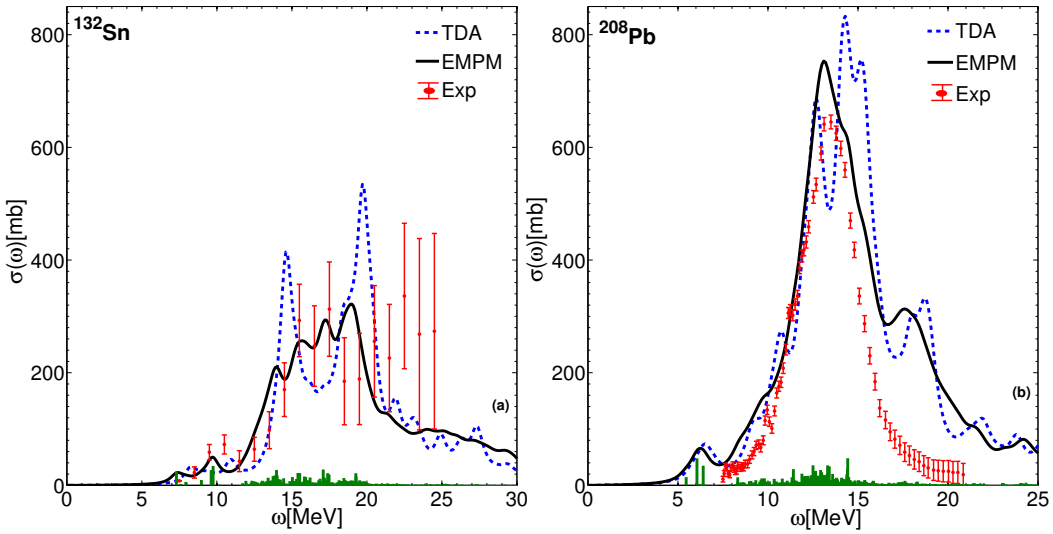

Figure 5.4: Experimental [70, 102] vs TDA and EMPM E1 cross section in ^{132}Sn (a) and ^{208}Pb (b). A Lorentzian of width Δ = 1 MeV is used. The vertical bars represent the EMPM cross section computed using the δ function as weight of the reduced strength in the Eq. (5.13).

strength

$$B_\nu(E1) = \langle \Psi_\nu \,||\, \mathscr{M}(E1) \,||\, \Psi_0 \rangle \,|^2, \tag{5.10}$$

where

$$\mathscr{M}(E1\mu) = \sum_i e_i r_i Y_{1\mu} \tag{5.11}$$

is the electric dipole operator. We have used the bare charges $e_i = e$ for protons and $e_i = 0$ for neutrons.

The $B(E1)$ strength is used to compute the dipole cross section

$$\sigma = \int_{E_0}^{E} \sigma(\omega) d\omega = \frac{16\pi^3}{9\hbar c} \int_{E_0}^{E} \omega S(E1,\omega) d\omega, \tag{5.12}$$

where $S(E1,\omega)$ is the $E1$ strength function,

$$S(E1,\omega) = \sum_{\nu} B_{\nu}(E1)\delta(\omega-\omega_{\nu}) \approx \sum_{\nu} B_{\nu}(E1)\rho_{\Delta}(\omega-\omega_{\nu}). \tag{5.13}$$

Here ω is the energy variable, ω_{ν} the energy of the transition from the ground to the ν_{th} excited state, and

$$\rho_{\Delta}(\omega-\omega_{\nu}) = \frac{\Delta}{2\pi}\frac{1}{(\omega-\omega_{\nu})^2+(\frac{\Delta}{2})^2} \tag{5.14}$$

is a Lorentzian of width Δ, which replaces the δ function as a weight of the reduced strength. The cross section is proportional to the classical energy weighted Thomas-Reiche-Kuhn (TRK) sum rule

$$S(TRK) = \sum_{n} \omega_n B_n(E1) = \frac{\hbar^2}{2m}\frac{9}{4\pi}\frac{NZ}{A}e^2. \tag{5.15}$$

We have in fact

$$\sigma = \frac{16\pi^3}{9\hbar c}S(TRK) = (2\pi^2)\frac{\hbar^2}{2m}\frac{e^2}{\hbar c}\frac{NZ}{A} = 60\frac{NZ}{A}(MeVmb). \tag{5.16}$$

The GDR exhausts more than 100% of the TRK sum rule. The contribution in excess comes from velocity dependent and exchange terms of the two-body nuclear potential.

The EMPM cross section for ^{132}Sn (Fig. 5.4(a)) is severely quenched and reshaped due to the one- to two-phonon coupling. It has a smoother behavior with respect to TDA and follows closely the experimental points. It has to be noticed however that the error bars are very large, especially in the high energy sector.

An analogous effect is caused by the one- to two-phonon coupling on the cross section of ^{208}Pb (Fig. 5.4(b)). The EMPM cross section is smoother than the TDA one and follows roughly the trend of the measured cross section.

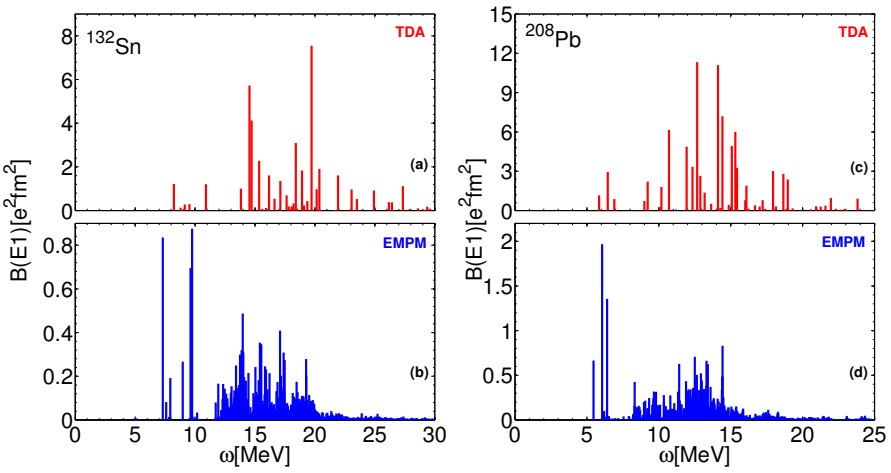

Figure 5.5: TDA (a, c) vs EMPM (b, d) E1 strength distribution in ^{132}Sn and ^{208}Pb.

An additional effect of the phonon coupling is the fragmentation of the strength. This effect, partly hidden in the cross sections due to the smoothing action of the Lorentzian, is clearly visible in the $E1$ spectra shown in Fig. (5.5). The strength splits into a low and a GDR sector in both TDA and EMPM. The EMPM spectra however are much more dense and are composed of peaks of considerably shorter height as compared to TDA in both the GDR and PDR regions.

This is visible for the PDR in Figs. (5.6) and (5.7), where a large number of weakly excited levels not present in TDA, appear. As shown in Figs. (5.8) and (5.9), these levels are excited by both the isoscalar and isovector operator suggesting their pygmy nature.

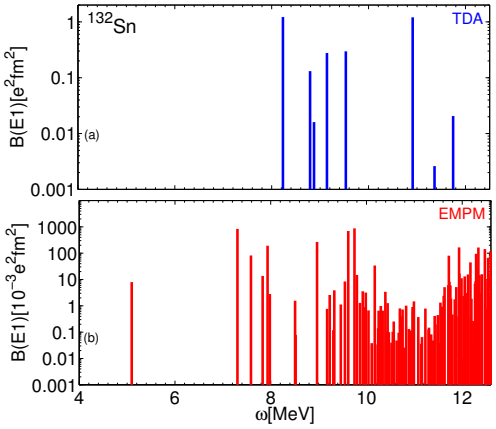

Figure 5.6: TDA (a) vs EMPM (b) E1 low-lying strength distribution.

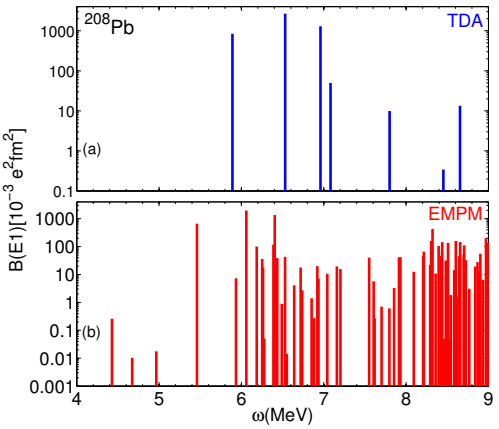

Figure 5.7: TDA (a) vs EMPM (b) E1 low-lying strength distribution.

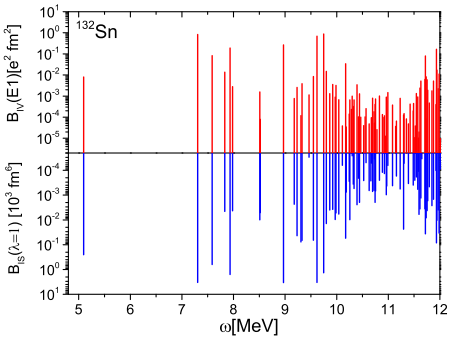

Figure 5.8: Isovector versus isoscalar E1 EMPM low-lying strength distribution in ^{132}Sn.

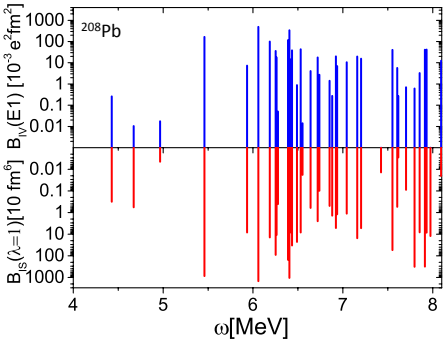

Figure 5.9: Isovector versus isoscalar E1 EMPM low-lying strength distribution ^{208}Pb.

5.4 Application of the EMPM to the neutron rich open shell ^{20}O

In order to describe the neutron rich open-shell ^{20}O we have to apply the method in the quasiparticle scheme. We adopt the intrinsic Hamiltonian (5.3). The density-dependent term V_ρ is unnecessary since $NNLO_{opt}$ reproduces well the experimental binding energies of light nuclei and oxygen isotopes.

The canonical HFB basis is generated in a configuration space which includes 11 harmonic oscillator major shells up to the principal quantum number $N_{max} = 10$. The TDA phonons are determined in a space which encompasses up to the (pfh) major shell. Their energy and structure remain practically unchanged if the two-quasiparticle space is further enlarged. The TDA phonons are free of spurious admixtures by virtue of the Gramm-Schmidt orthogonalization of the two-quasiparticle states to the c.m. and the particle-number states (Sect. 3.4).

The correlated two-phonon states $\mid \alpha_2\rangle$ are generated in a space truncated according to the energy $(E_{\lambda_1} + E_{\lambda_2})$ of the basis states $\mid (\lambda_1 \times \lambda_2)^\beta\rangle = \{O^\dagger_{\lambda_1} \times \mid \lambda_2)\rangle\}^\beta$. They are added to the HFB vacuum plus the TDA one-phonon basis to solve the full eigenvalue equations determining the ground and excited EMPM states.

The ground-state correlation energy depends critically on the truncation of the two-phonon space. If we use the full two-phonon basis allowed by the number of shells up to the (pf h) shell the ground state gets severely depressed. As already discussed before, this energy shift would be counterbalanced by the inclusion of three phonons. Including so many three phonon states, however, would require unbearably lengthy calculations unless we resort to some efficient approximations.

We therefore confine our calculation to the two-phonon space and consider the space truncation energy cutoff as a parameter to be fixed so as to reproduce roughly the first excited 1^- level. This is achieved by including two-phonon states composed of all TDA phonons fulfilling the condition $(E_{\lambda_1} + E_{\lambda_2}) = 30$ MeV.

The TDA and EMPM level schemes are compared to the experimental spectrum [103] in Fig. (5.10). The crucial role played by the two-phonon states emerges clearly from the plot. The TDA spectrum is far from resembling the experimental one. Once the two phonons are included, the calculation yields a sequence of levels which follow fairly close the experimental scheme, although some discrepancies still remain. The two-phonon affect strongly also the $E1$ response. As shown in Fig. (5.11), the strength gets fragmented and quenched by the phonon coupling. Of special interest is the splitting of the low-lying TDA peak into several smaller peaks with the appearance of two levels below the neutron decay threshold, in agreement with the data obtained in [105]. As shown in Fig. (5.11 (c)), the strengths of these two levels are in good agreement with experimental data. These levels contribute to the small hump in the cross section at low-energy shown in Fig. (5.12). This can be associated to the PDR in ^{20}O. In fact, as shown in (Tab. 5.1), the lowest TDA phonons have an overwhelming predominance of neutron components.

At high energy, some discrepancies between theoretical and experimental cross section appear. It is underestimated in the region $8-12$ and $14-18$ MeV. In fact the strength collected by the states up to ~ 15 MeV is $\sim 6\%$ of TRK sum rule, while the experimental one is $\sim 12\%$. The total strength also is underestimated. The theoretical integrated cross section up to ~ 27 MeV is the $\sim 38\%$ to be compared with the $\sim 45\%$ fraction exhausted by the experimental data.

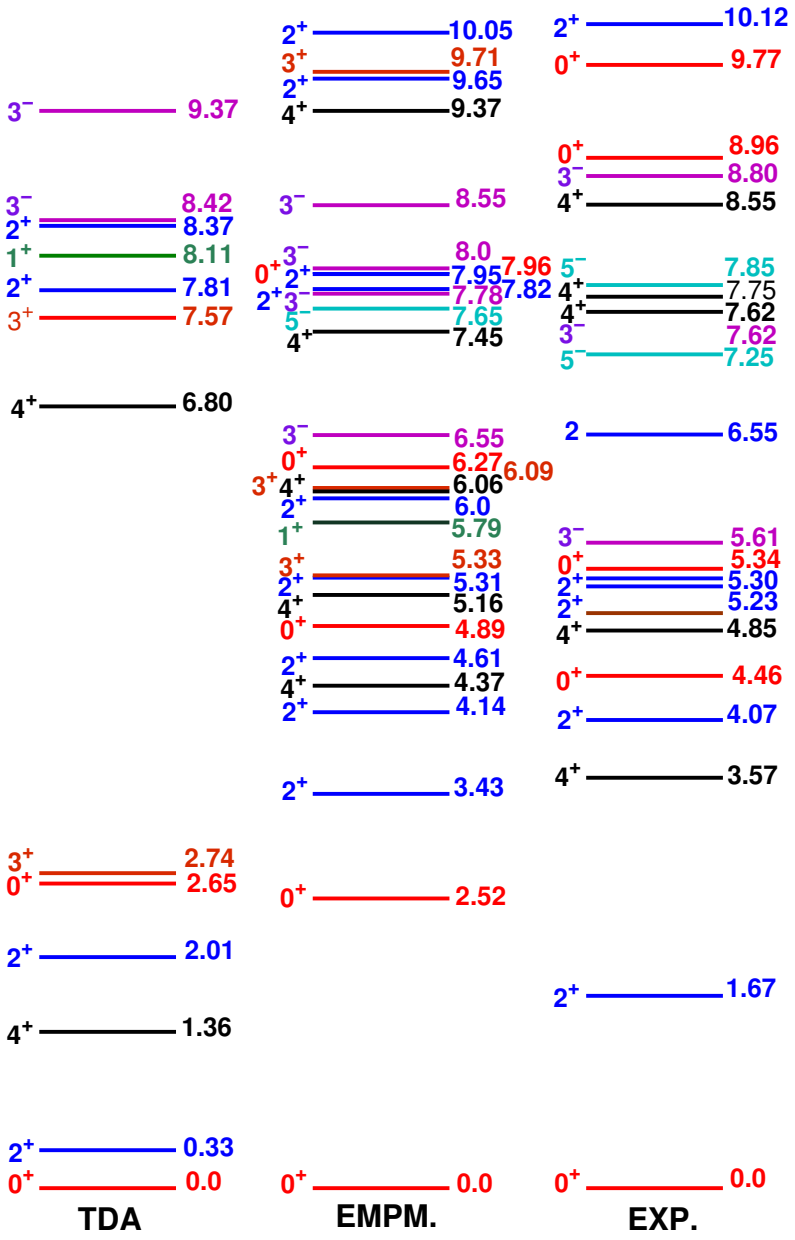

Figure 5.10: Theoretical versus experimental [103] level scheme of ^{20}O.

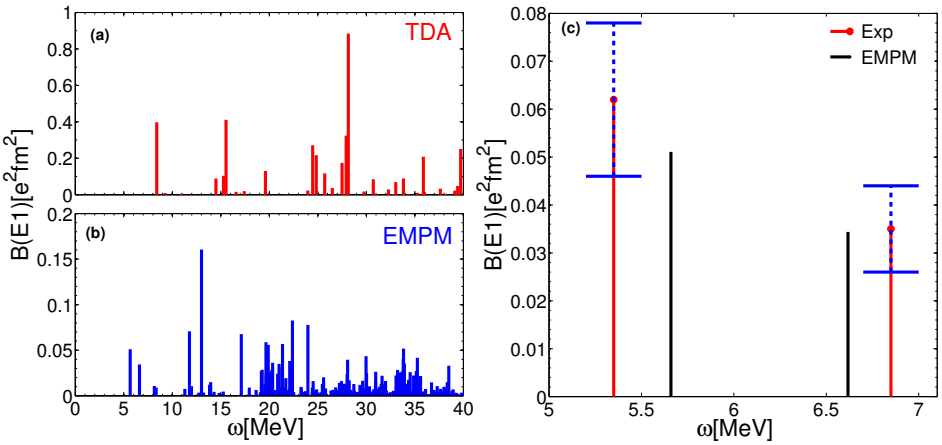

Figure 5.11: $E1$ strength distribution within TDA (a), EMPM (b) and comparison with experimental data [104] of the two lowest levels in ^{20}O

Table 5.1: Proton (π) and neutron (ν) two-quasiparticle composition of the 1^- TDA phonon of energy $\omega = 8.397$.

$r_\pi s_\pi$	c^π_{rs}	$r_\nu s_\nu$	c^ν_{rs}
$0d_{5/2}0p_{3/2}$	-0.188	$0d_{5/2}0p_{3/2}$	-0.174
$0d_{3/2}0p_{3/2}$	-0.053	$1s_{1/2}0p_{3/2}$	0.102
$0d_{3/2}0p_{1/2}$	0.117	$0d_{3/2}0p_{1/2}$	0.117
$1d_{3/2}0p_{1/2}$	-0.063	$0d_{5/2}1p_{3/2}$	0.718
		$1s_{1/2}1p_{3/2}$	-0.505
		$1s_{1/2}1p_{1/2}$	0.192
		$0d_{3/2}1p_{1/2}$	0.119
		$0d_{5/2}0f_{7/2}$	0.160
		$0d_{5/2}1f_{7/2}$	0.075

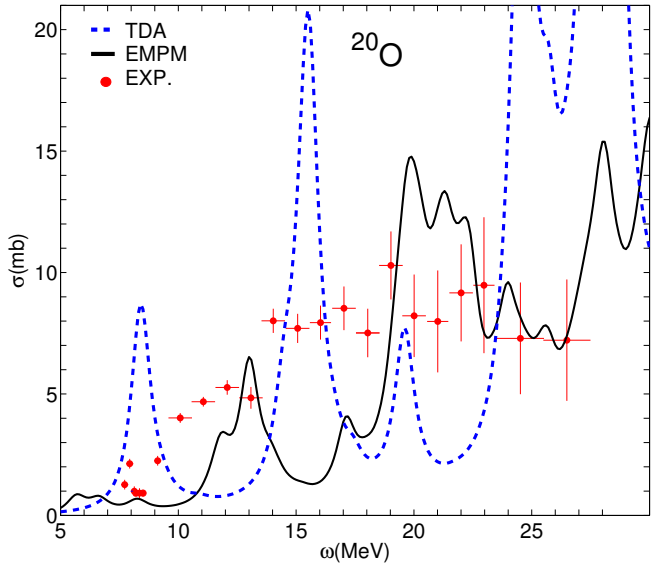

Figure 5.12: Theoretical versus experimental $E1$ cross section in ^{20}O. We have used a Lorentzian of width $\Delta = 1$MeV

Chapter 6

Application of the EMPM to odd-even nuclei: ^{17}O and ^{17}F

For the odd mass nuclei we have used the intrinsic Hamiltonian (5.3) to generate the HF basis in a configuration space including up to the $N_{max} = 15$ harmonic oscillator major shell. The TDA phonons are derived from a subset of HF states corresponding to $N = 12$. Their structure does not change if we used the full HF space. The multiphonon particle-core basis is composed of a) all one-phonon particle-core states $|\,(p \times \alpha_1)^{\nu}\rangle$; b) the two-phonon $|\,(p \times \alpha_2)^{\nu}\rangle$ of energies $E_{\alpha_2} \leq 35$ MeV; c) the three-phonon $|\,(p \times \alpha_3)^{\nu}\rangle$ of energies $(\varepsilon_p + E_{\alpha_3}) \leq 55$ MeV.

The inclusion of the three-phonon particle-core states has required some approximations. We ignored the interaction $\mathscr{V}_{p\alpha_3,p'\alpha_3'}$ (4.60) in the eigenvalue equation (4.59) and neglected the phonon-phonon potential (4.15) $\mathscr{V}_{\lambda\alpha,\lambda'\alpha}$ in the Eq. (4.17) determining the core states $|\,\alpha_3\rangle$. We have also neglected the exchange terms between the odd particle and $|\,\alpha_3\rangle$ by putting $\mathscr{D}_{p\alpha_3,p'\alpha_3'} = \delta_{pp'}\delta_{\alpha_3\alpha_3'}$ in the Eq. (4.58).

The lack of antisymmetrization between the odd particle and the three-phonon core states may yield some linear dependence among the $|\,(p\times\alpha_3)^{\nu}\rangle$ states and might overestimate their couplings to the one-phonon and two-phonon particle-core components. The other two approximations affect the energy distribution of states lying at high energies and, therefore, do not have appreciable consequences.

6.1 Spectra

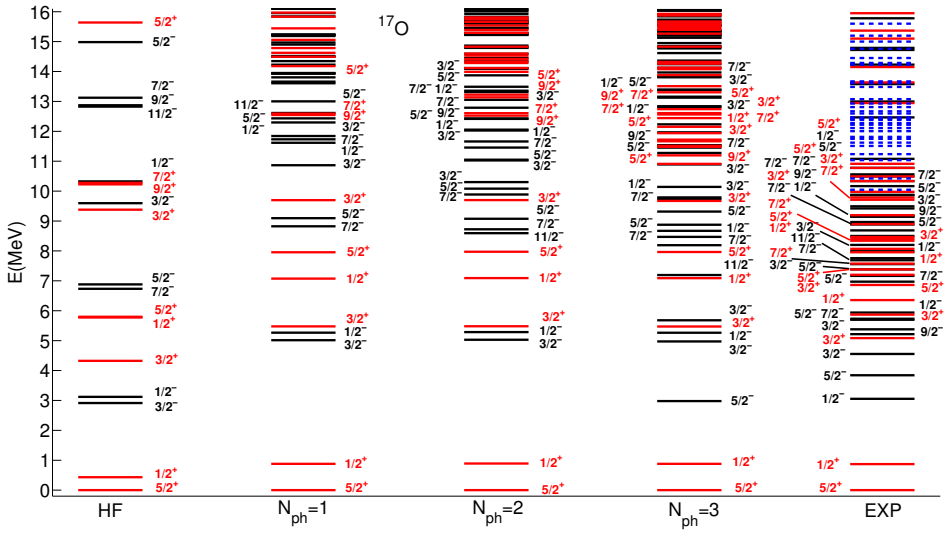

Figure 6.1: Theoretical versus experimental spectra in ^{17}O. N_{ph} indicates the maximum phonon number. The dashed levels have unknown spin or parity or both.

The theoretical spectra obtained for ^{17}O and ^{17}F in different multiphonon spaces are compared to one another and with experiments in Fig. (6.1) for ^{17}O and in Fig. (6.2) for ^{17}F. The phonon compositions of the selected eigenstates are reported in Table (6.1).

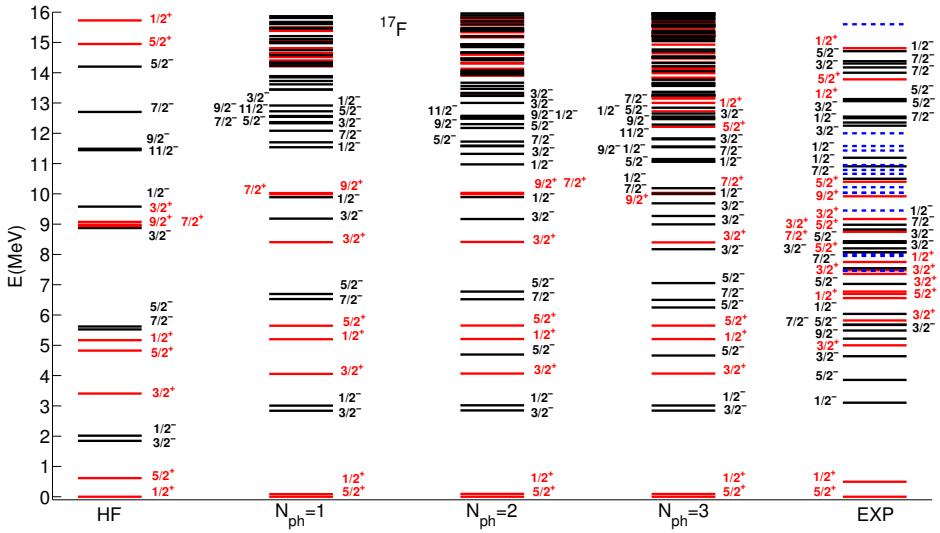

Figure 6.2: Theoretical versus experimental spectra in ^{17}F. N_{ph} indicates the maximum phonon number. The dashed levels have unknown spin or parity or both.

The one-phonon states alter appreciably the HF levels. They depress the lowest $5/2^+$ with respect to the other states thereby enhancing its distance from the other levels.

In ^{17}O this energy shift is beneficial for the low-lying positive parity levels, especially the $1/2^+_1$ and $3/2^+_1$, which get closer to the experimental levels of single particle nature. The negative parity states, instead, get pushed at too high energies with the exception of the $3/2^-_1$.

In ^{17}F the energy shift promotes the inversion between the $1/2^+_1$ and $5/2^+_1$ levels, and therefore yields the correct ground state. Due to the more pronounced depression of the $5/2^+$state, the other low-lying levels appear at higher energies in better overall agreement with the experiments.

Table 6.1: Phonon composition of selected states $|\Psi_\nu\rangle$ in ^{17}O and ^{17}F.

	J^ν_π	E^ν	$\lvert C^\nu_0\rvert^2$	$\lvert C^\nu_1\rvert^2$	$\lvert C^\nu_2\rvert^2$	$\lvert C^\nu_3\rvert^2$
^{17}O	$\frac{5}{2}^+_1$	0.0000	0.9510	0.0484	0.0005	0.0001
	$\frac{1}{2}^+_1$	0.8808	0.9408	0.0586	0.0002	0.0004
	$\frac{5}{2}^-_1$	2.9796	0.0003	0.7500	0.0120	0.2377
	$\frac{3}{2}^-_1$	4.9733	0.8855	0.0942	0.0021	0.0182
	$\frac{1}{2}^-_1$	5.2635	0.9787	0.0198	0.0001	0.0014
	$\frac{3}{2}^+_1$	5.4730	0.9457	0.0535	0.0004	0.0004
	$\frac{11}{2}^-_1$	7.1942	0.0006	0.8822	0.0752	0.0420
	$\frac{7}{2}^-_1$	8.1929	0.4278	0.4856	0.0195	0.0671
	$\frac{1}{2}^-_2$	8.4706	0.0171	0.8459	0.0108	0.1262
	$\frac{9}{2}^+_1$	10.9115	0.0074	0.8290	0.0944	0.0692
	$\frac{9}{2}^-_1$	11.5319	0.0005	0.9342	0.0345	0.0308
	$\frac{7}{2}^+_1$	11.9392	0.0081	0.8449	0.0680	0.0790
^{17}F	$\frac{5}{2}^+_1$	0.0000	0.9647	0.0351	0.0002	0.0000
	$\frac{1}{2}^+_1$	0.0892	0.9675	0.0323	0.0001	0.0001
	$\frac{3}{2}^-_1$	2.8437	0.9899	0.0098	0.0001	0.0002
	$\frac{1}{2}^-_1$	3.0131	0.9897	0.0100	0.0000	0.0003
	$\frac{3}{2}^+_1$	4.0666	0.9796	0.0203	0.0000	0.0001
	$\frac{5}{2}^-_1$	4.6630	0.0215	0.7483	0.0220	0.2082
	$\frac{1}{2}^+_2$	5.2050	0.9721	0.0277	0.0001	0.0001
	$\frac{7}{2}^-_1$	6.4988	0.9740	0.0244	0.0008	0.0008
	$\frac{1}{2}^-_2$	9.6875	0.5268	0.4416	0.0032	0.0284
	$\frac{9}{2}^+_1$	9.9913	0.9859	0.0137	0.0003	0.0001
	$\frac{7}{2}^+_1$	10.0325	0.9866	0.0131	0.0002	0.0001
	$\frac{9}{2}^-_1$	11.5656	0.0030	0.9400	0.0300	0.0270
	$\frac{11}{2}^-_1$	11.8336	0.0061	0.8985	0.0510	0.0444

The inclusion of the one-phonon states enrich greatly the spectra by generating a large number of levels. Unfortunately these new states fall at too high energies ($\geq 11MeV$) with respect to the corresponding experimental levels. This high-energy states are not affected by two-phonon states which contributes only to enrich further the high-energy region. Only the three phonons, by pushing few negative parity states down in energy, enrich the low-energy spectra but not sufficiently to reproduce the experimental density.

6.2 Moments and transitions

6.2.1 Magnetic moment and β-decay ft value

The magnetic moments have been computed starting from the magnetic operator

$$\vec{\mu} = \sum_k \left(g_l(k)\vec{l}_k + g_s(k)\vec{s}_k \right), \tag{6.1}$$

whith the bare gyromagnetic factors given by

$$g_l^p(k) = 1, g_s^p(k) = 5.59, \tag{6.2}$$

$$g_l^n(k) = 0, g_s^n(k) = -3.83. \tag{6.3}$$

The β decay log ft value is defined by

$$ft_{1/2} = \frac{\kappa}{(B_F + B_{GT})}, \tag{6.4}$$

with $\kappa = 6147$. The B_F and B_{GT} are the reduced Fermi and Gamow-Teller strengths

respectively, given by

$$B_F(i \to f) = \frac{g_v^2}{[J_i]} \mid \langle f, Jf \mid\mid M_F \mid\mid i, J_i \rangle \mid^2, \tag{6.5}$$

$$B_{GT}(i \to f) = \frac{g_A^2}{[J_i]} \mid \langle f, Jf \mid\mid M_{GT} \mid\mid i, J_i \rangle \mid^2 . \tag{6.6}$$

The Fermi and Gamow-Teller operators are defined as

$$M_F = \sum_{rs} \langle r \mid\mid 1 \mid\mid s \rangle \left(a_r^\dagger \times b_s \right)^0 = \sum_r [r]^{1/2} \left(a_r^\dagger \times b_s \right)^0, \tag{6.7}$$

$$M_{GT} = \frac{1}{\sqrt{(3)}} \sum_{rs} \langle r \mid\mid \sigma \mid\mid s \rangle \left(a_r^\dagger \times b_s \right)^1, \tag{6.8}$$

with the bare weak charges $g_v^2 = 1.0$, $g_A^2 = 1.25$. The results, compared with experimental data [106], are shown in table (6.2).

The magnetic moments in both ^{17}O and ^{17}F are practically determined at the HF level. The weak quenching due to the core brings the total moments slightly more distant from the experimental values. It may be worth to point out that the core contribution originates from the spin-flip partners present in the HF p-h configurations entering the TDA phonons and, therefore, is ultimately ascribed to HF.

The β-decay is also ruled by HF. Indeed, the ft value comes almost entirely from the transition between the HF components of the $5/2^+$ ground states of both nuclei (Tab.6.2). The weak quenching caused by the phonon coupling brings the ft value slightly above the measured quantity.

Table 6.2: Ground state magnetic μ, electric quadrupole Q moments, $B(E\lambda;J_i^\pi \to J_f^\pi)(e^2fm^{2\lambda})$ and log ft value. The experimental values are taken from [106]. The sign of the experimental quadrupole moment of ^{17}F is not known.

		HF	EMPM	Exp
^{17}O	$\mu(\mu_N)$	-1.91	-1.83	-1.89
	$Q(efm^2)$	0	-0.841	-2.578
	$B(E2;5/2_1^+ \to 1/2_1^+)$	0	0.17	2.18(16)
	$B(E1;5/2_1^+ \to 5/2_1^-)$	0.0083	0.0042	0.0004
	$B(E1;5/2_1^+ \to 1/2_1^-)$	0.482	0.249	0.0005
	$B(E1;5/2_1^+ \to 1/2_2^-)$	0.0173	0.0005	
^{17}F	$\mu(\mu_N)$	+4.79	+4.63	+4.72
	$Q(efm^2)$	-9.9	-7.6	5.8(4)
	$B(E2;5/2_1^+ \to 1/2_1^+)$	40.71	21.89	21.64
	$B(E1;5/2_1^+ \to 5/2_1^-)$	0.015	0.0004	0.0018
	$B(E1;5/2_1^+ \to 1/2_1^-)$	0.60	0.40	0.0006
	$B(E1;5/2_1^+ \to 1/2_2^-)$	0.087	0.0265	
	$B(E1;5/2_1^+ \to 1/2_3^-)$	0.000	0.0013	
	logft	3.294	3.391	3.358(2)

6.2.2 Electric quadrupole moments and low-lying transitions

The quadrupole moment and the $E2$ transitions have been computed by using the operator

$$\mathscr{M}(E\lambda\mu) = \sum_i e_i r_i^\lambda Y_{\lambda\mu}, \tag{6.9}$$

with $\lambda = 2$ and bare charges $e_p = e$ and $e_n = 0$.

The absolute value of the quadrupole moment is underestimated in ^{17}O by a factor three and the $E2$ strength of the transition from the ground state $5/2^+_1$ to $1/2^+_1$ is underestimate by an order of magnitude (Tab 6.2). Since the odd particle is a neutron, and the the states $5/2^+_1$ and $1/2^+_1$ have single particle nature (Tab. 6.1), the contribution to the moments and transition strength comes entirely from the terms $M_{01}(E2)$ (4.71) and $M_{10}(E2)$ (4.72) which couple the single particle components of $5/2^+_1$ and $1/2^+_1$ to the $\lambda = 2^+$ particle-phonon pieces of $1/2^+_1$ and $5/2^+_1$, respectively.

In ^{17}F the quadrupole moment, computed in HF, is ~ 1.7 times the measured value. It gets considerably smaller and closer to experiments once the phonon coupling is included.

The coupling is even more effective on the $5/2^+_1 \rightarrow 1/2^+_1$ $E2$ transition. Once the phonon are included, the $E2$ strength, wich is ~ 1.8 times larger in HF, gets considerably reduced and coincides in practice with the experimental value (Tab 6.2).

The strong effect of the phonon coupling in ^{17}F seems to clash with the analysis made for the ^{17}O, especially since the HF components of $5/2^+_1$ and $1/2^+_1$ in ^{17}F are even more dominant than in ^{17}O (Tab. 6.2). However the inconsistency is only apparent. In fact, the large effect on the $B(E2)$ in ^{17}F comes from the indirect coupling among different single particle components of the ground state wave function. The phonons, in fact, not only get admixed directly with the HF components, but combine the HF states among themselves. It follows that the single particle piece of each wavefunction $|\Psi_\nu\rangle$ is a linear combination of different HF configurations. Their mutual interference causes the quenching of quadrupole moment and transition in ^{17}F. In ^{17}O, this interference has no effect since the odd

neutron carries no charge.

6.2.3 Low-lying $E1$ transitions

We have computed the $E1$ transitions using the intrinsic operator referred to the CM coordinate. This keeps the form (6.9) with $\lambda = 1$ and effective charges $e_p = (N/A)e$ and $e_n = (Z/A)e$. The effective charges do not affect the TDA core states, which are free of CM spurious admixtures by virtue of the Gramm-Schmidt orthogonalization method outlined already (Sect. 3.4). It modifies, instead, the single-particle contributions, especially the transitions between states of dominant single particle character.

The $B(E1;5/2^+ \to 5/2^-)$ value in the ^{17}O (Tab. 6.2), though small, is an order of magnitude larger than the experimental value. The $5/2^-$ state involved is an intruder (Tab. 6.1), without a corresponding HF state, with a dominant particle-phonon component. Thus, the larger strength, coming from the core excitation, suggests that the particle-phonon component of this state is too large.

The $E1$ transition connecting the two states of single particle nature $1/2^+_1$ to $1/2^-_1$ is much larger then the experimental one. This is, instead, reproduced by the strength of the transition to $1/2^-_2$. This suggests that this state could be associated to the first experimental $1/2^-$, but it lies at too high energy. A more effective phonon coupling could push down this state and produce an energy crossing between the two lowest $1/2^-$ states.

The $E1$ transition from the ground state $5/2^+_1$ to $5/2^-_1$ in ^{17}F is underestimated. This effect is due to a partial cancellation of the single particle ($M_{00} = -0.039$ efm) and particle-phonon ($M_{01} = 0.020$ efm, $M_{10} = 0.001$ efm) contributions. The single particle contribution, negligible in ^{17}O, is comparable to the one

induced by the core excitation in ^{17}F. The reason of such a difference is due to the larger amplitudes of the single-particle components of both $5/2^+_1$ and $5/2^-_1$ in ^{17}F (Table 6.1) with respect to ^{17}O .

The $E1$ transition connecting $1/2^+_1$ to $1/2^-_1$ in ^{17}F is largely overestimated as in ^{17}O. This is due to the large single particle contribution ($M_{00} = 0.900$ efm). This is not the case of the $E1$ transition to $1/2^-_2$ and $1/2^-_3$. It would therefore plausible to associate such a state to the lowest experimental $1/2^-$ level, if a crossing between the $1/2^-_3$ and $1/2^-_1$ levels could be achieved by a stronger particle-phonon coupling.

6.3 Electric dipole response

We start with the investigation of the dipole response in ^{16}O. As shown in Fig. (6.3 (a)), the TDA cross section is displaced slightly upward in energy with respect to experiments. The action of the two phonons is weak. The three phonons, instead, affect strongly the cross section, which gets shifted downward and peaked in the right position. The shape of the cross section is not so distant from the one resulting from the measurements. The two main peaks, for instance, are reproduced fairly well. Each of them arises mainly from a strong transition to a single TDA state. The other secondary peaks are also due mainly to single transitions.

In ^{17}O, the dipole cross section gets displaced upward in energy by the coupling of the odd particle to the TDA phonons. Its main peak is too high and lies several MeV above the experimental one (Fig. 6.3 (b)).

As in ^{16}O (Fig. 6.3 (a)), the cross section gets damped and down-shifted mainly by the couplings to three phonons. The peak, however, is still to high and

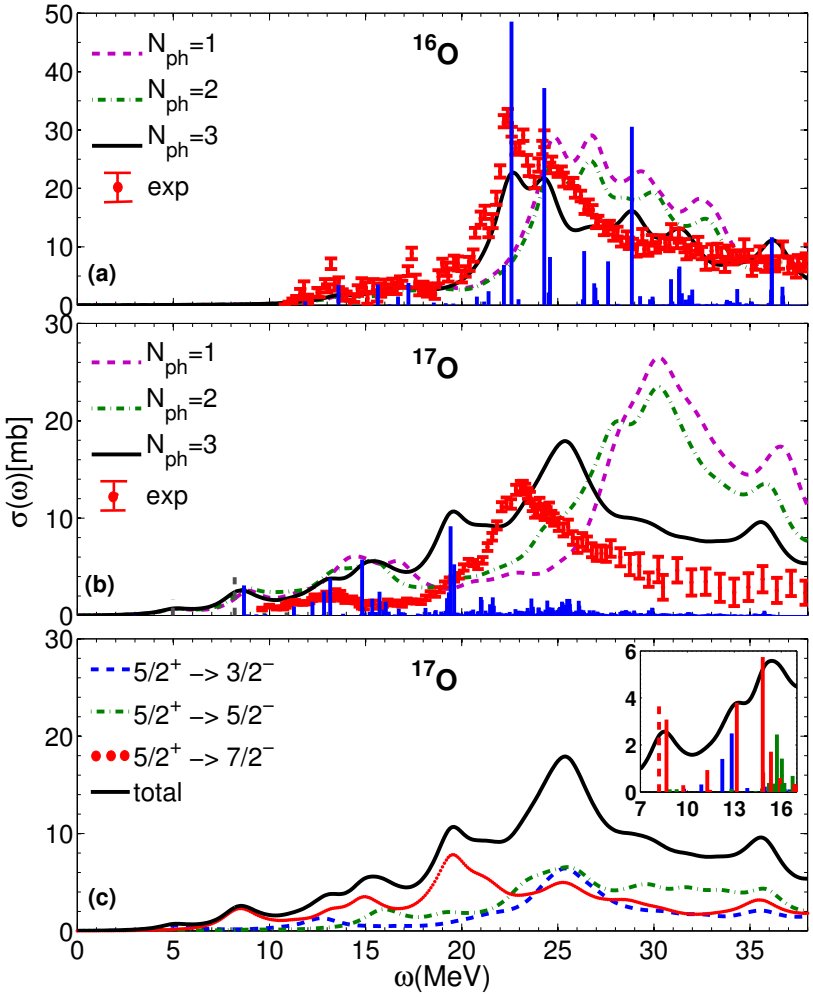

Figure 6.3: The theoretical $E1$ cross sections, computed in different multiphonon spaces, are compared with the experimental ones in ^{16}O (a) and ^{17}O (b). The data are taken from [107] for ^{16}O and from [108] for ^{17}O. A Lorentzian of width $\Delta = 2$ MeV is used. The vertical bars represent the $N_{ph} = 3$ cross section computed using the δ function as weight of the reduced strength in the Eq. (5.13). The dashed bars denote the transitions of single particle character. The separate contributions of the $3/2_i^-$, $5/2_i^-$, and $7/2_i^-$ excitations to the $E1$ cross section in ^{17}O are shown in plot (c). The red bars in the inset refer to the $5/2^+ \rightarrow 7/2^-$ transitions.

~ 2 MeV above in energy.

The effect of the large $E1$ strength carried out by single particle transition on the cross section is shown in Figs. (6.3) and (6.4), were the strength connecting states with dominant single particle contribution are in dotted bars. They, being in the low-energy sector, do not alter appreciably the cross sections.

Important differences between ^{16}O and ^{17}O emerge however from the analysis of the integrated cross section. The experimental cross section integrated up to 40 MeV over-exhausts the TRK sum rule by a factor ~ 1.26 in ^{16}O, to be compared with the computed fraction of $\sim 100\%$. In ^{17}O, the theoretical integrated cross section accounts for $\sim 98\%$ of the TRK sum rule, while the fraction exhausted by the data is $\sim 50\%$. An appreciable share goes to the region of the pygmy resonance. The strength integrated up to $\omega \leq 15$ MeV exhausts $\sim 9\%$ of the TRK sum rule, three times the measured value $\sim 3.2\%$.

A better understanding of the excitation mechanism is gained by investigating the strength distribution. From comparing the TDA spectrum of ^{16}O (Fig. 6.5 (a)) with the corresponding one in ^{17}O (Fig. 6.5 (b)) one notices that adding an odd particle to the core induces a huge damping and fragmentation. Such an effect was largely expected, since the strength collected by each 1^- core state gets distributed among several states of spin $3/2^-$, $5/2^-$, and $7/2^-$ (Fig. 6.6).

The main peak of the theoretical cross section (Fig. 6.5 (b)) arises from a bunch of closely packed weakly excited levels around ~ 25 MeV. As the plots in Fig. (6.6) show, all three $3/2^-$, $5/2^-$, and $7/2^-$ states carry strength in this region and, therefore, contribute to the main peak on equal footing (Fig. 6.3 (c)).

The unwanted secondary peak at ~ 20 MeV (Fig. 6.5 (b)) originates mostly from the strong transitions to the $7/2^-$ states at the same energy (Fig. 6.6 (c)). At

low energy, we can distinguish four small humps (Fig. 6.3 (c)). The small one at ~ 5 MeV comes from the excitation of the single-particle $3/2^-$ state (Fig. 6.6 (a)), the one within $5-10$ MeV is due to the two $7/2^-$ states at ~ 8 MeV (Fig. 6.6 (c)), the lowest one being of single particle nature. Also the two peaks around ~ 12.5 MeV and ~ 15 MeV arise mostly from exciting few $7/2^-$ states (inset of Fig. 6.3 (c)) with a small contribution of $3/2^-$ states (Fig. 6.6 (a)) to the first peak and of $5/2^-$ excitations (Fig. 6.6 (b)) to the second.

The phonon action in ^{17}F is analogous to the one exerted in ^{17}O. The cross section gets quenched and shifted mainly by the coupling to three phonons (Fig. 6.4 (a)), but its behavior is smoother than in ^{17}O. We get, in fact, a broad wiggly hump, covering a wide energy range ($20-40$ MeV), which arises from a huge numbers of closely packed small peaks.

Strong transitions are predicted at energies ≤ 15 MeV (Fig. 6.7(c)). The lowest four are due to single particle excitations and yield the lowest three humps in the cross section (Fig. 6.4 (b)). The fourth hump in the $13-15$ MeV interval originates almost entirely from the excitation of $7/2^-_3$ with small contributions of other weak transitions, including $5/2^+_1 \rightarrow 7/2^-_4$ (inset of Fig. 6.4 (b)). It is likely to correspond to the pygmy resonance, which, according to the experimental analysis of Ref. [106], is due to the excitation of two 7/2? states. It accounts for $\sim 2\%$ of TRK sum rule. The integrated cross section in ^{17}F up to ~ 40 MeV exhausts $\sim 81\%$ of the sum.

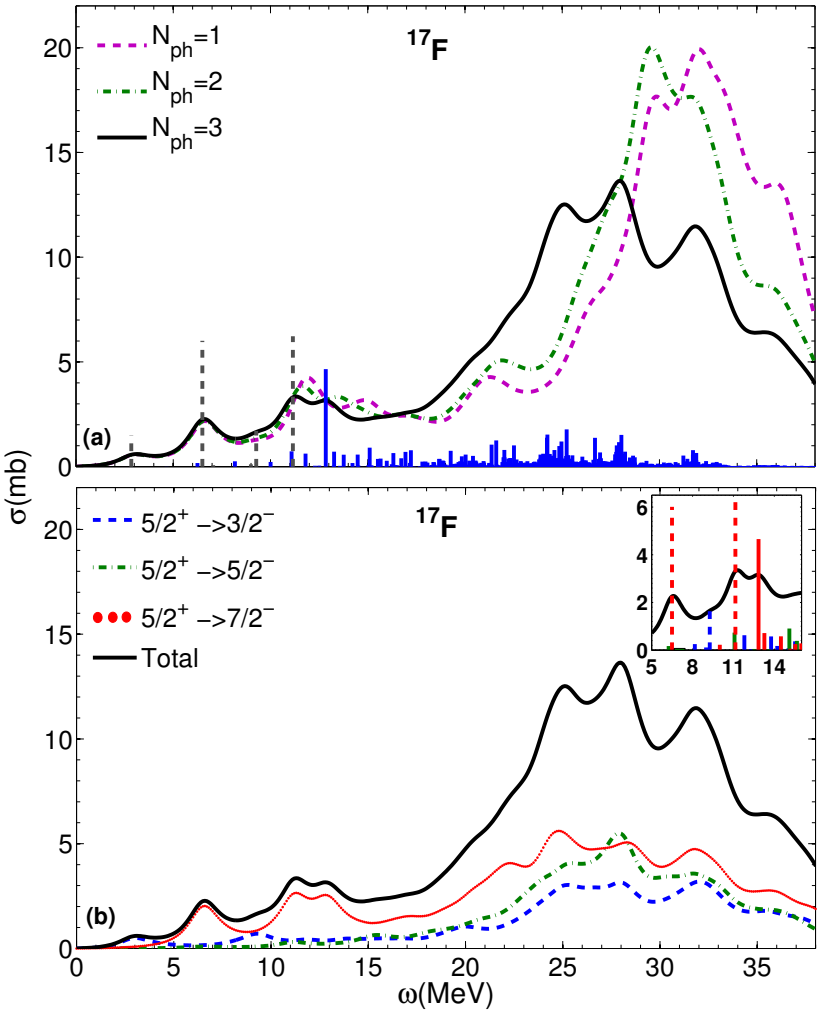

Figure 6.4: The theoretical $E1$ cross sections, computed in different multiphonon spaces, are compared in ^{17}F (a). A Lorentzian of width $\Delta = 2$ MeV is used. The vertical bars represent the $N_{ph} = 3$ cross section computed using the δ function as weight of the reduced strength in the Eq. (5.13). The dashed bars denote the transitions of single particle character. The separate contributions of the $3/2^-_i$, $5/2^-_i$, and $7/2^-_i$ excitations to the $E1$ cross section in ^{17}F are shown in plot (b). The red bars in the inset refer to the $5/2^+ \rightarrow 7/2^-$ transitions.

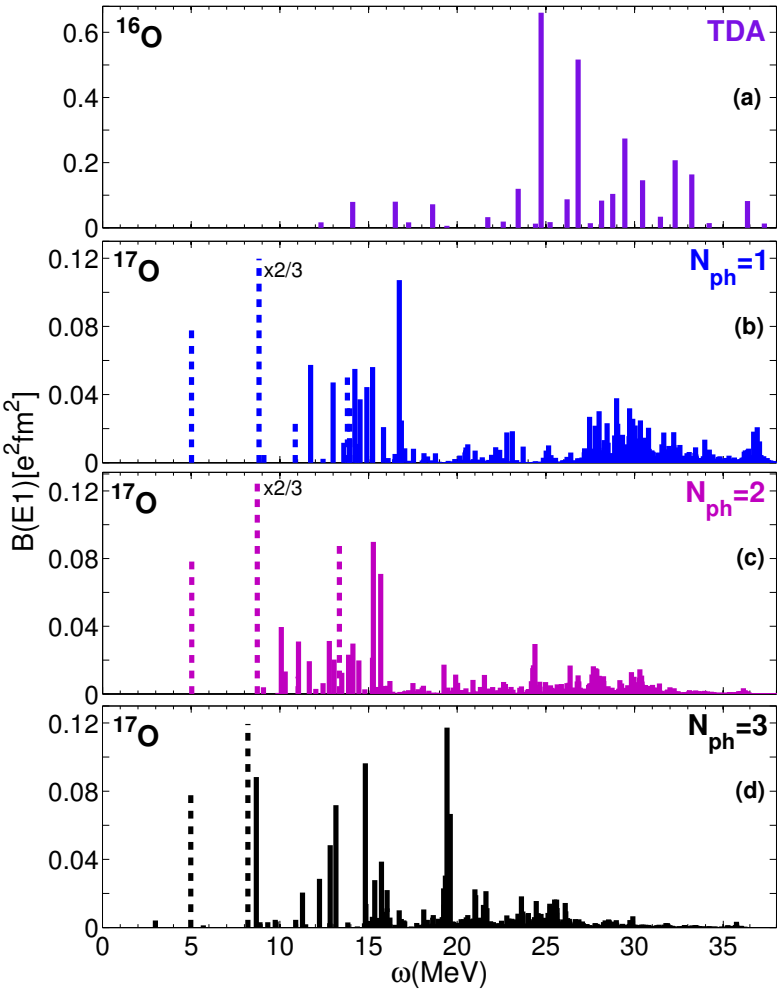

Figure 6.5: $E1$ strength distribution of ^{17}O computed in spaces including up to $N_{ph} = 1$(b), $N_{ph} = 2$ (c), and $N_{ph} = 3$ (d) phonons. The dashed bars denote the transitions of single particle character. The TDA spectrum of ^{16}O (a) is also shown for comparison. A different scale is used for the latter plot.

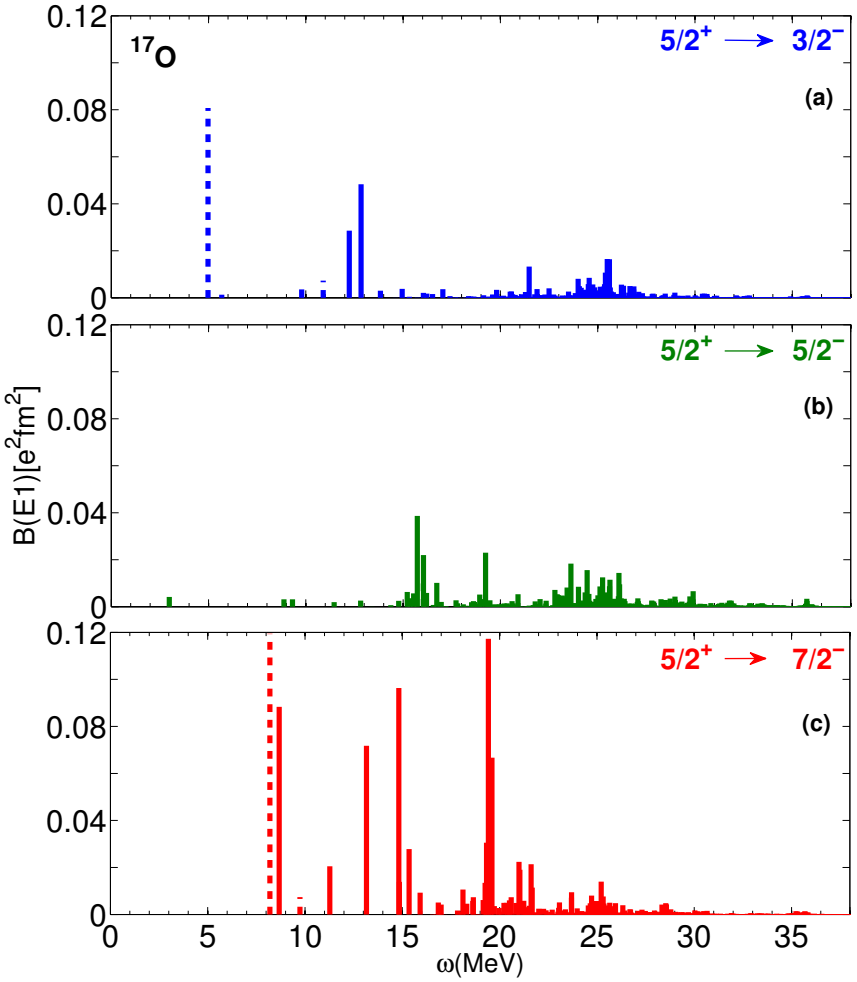

Figure 6.6: $E1$ strength distribution of the transitions to $3/2_i^-$(a), $5/2_i^-$ (b), and $7/2_i^-$ (c) in ^{17}O. The dashed bars denote the transitions of single particle character.

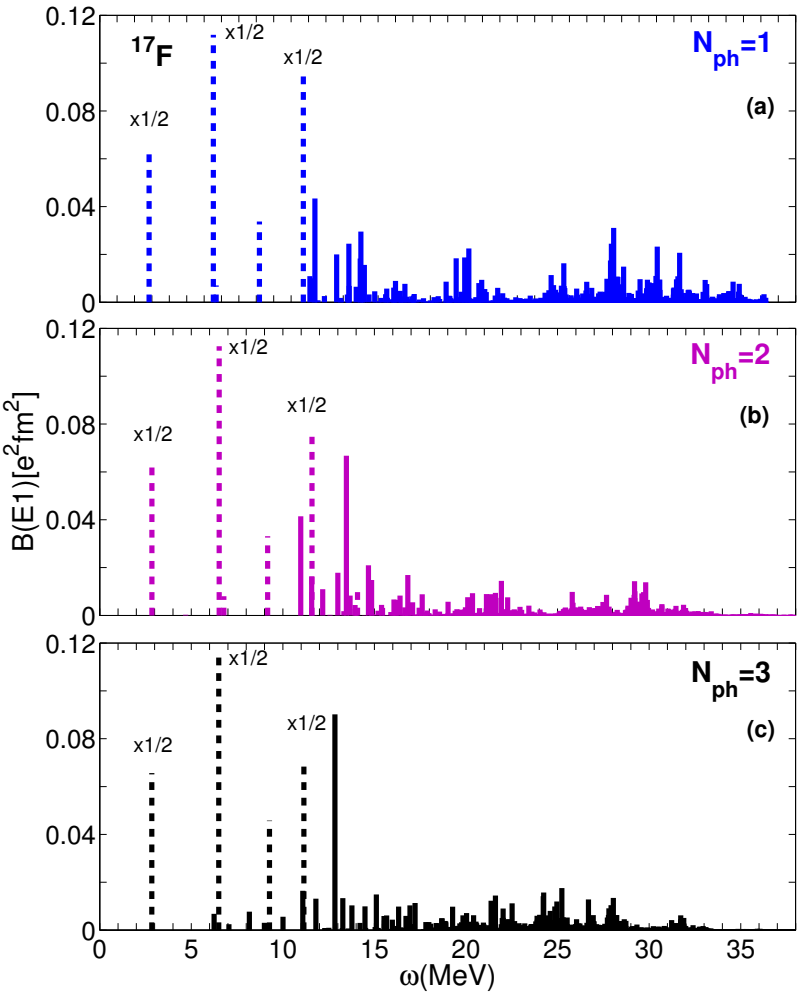

Figure 6.7: $E1$ strength distribution of ^{17}F computed in spaces including up to $N_{ph} = 1$(a), $N_{ph} = 2$ (b), and $N_{ph} = 3$ (c) phonons. The dashed bars denote the transitions of single particle character.

Conclusions

In even-even nuclei, the inclusion of a subset of the two-phonon basis states enhances the density of levels and fragments strongly the dipole strength computed in TDA. The strong depression of the correlated ground state induced by the coupling of the HF vacuum to the two-phonon basis induces an unrealistic large gap between ground and excited levels. More complex configurations, chiefly four-phonon states, are needed. This is suggested also by CC-theory calculations which take effectively into account (4p-4h) configurations and reproduce the ground-state energies [109]. We have shown, indeed, that, even when all two-phonon states are included, the binding energy per nucleon approaches but does not reach the experimental values [110].

Unlike the ground state, the one-phonon excited states are insensitive to the dimensions of the two-phonon space. It would be necessary to include the three-phonon states in a space large enough to restore the correct separation between excited and ground energy levels. These configurations are known to couple strongly to the one-phonon states and to push them down in energy [20]. Since these complex configurations are not included in our calculation, we referred the energies to the unperturbed HF ground state or to a correlated ground state obtained by an appropriate truncation of the 2-phonon space.

In odd-even nuclei, the one-phonon states, through their coupling, improve the description of the low-lying states of single particle nature. These new states enrich greatly the spectra but remain at too high energy with respect to the experimental levels. The two-phonon states enrich further the high-energy sector and get admixed with one-phonon states. Only the three phonon states push down in energy few one-phonon states through their strong coupling and enrich the low-energy sector in qualitative partial agreement with experiments.

The three phonons exert a crucial quenching action on the $E1$ transitions. They reduces substantially the gap between the theoretical and experimental $E1$ cross sections. However, sizable discrepancies remain. The damping and energy shift, though appreciable, are not sufficient to reproduce completely peak, shape and magnitude of the cross section in ^{17}O.

The magnetic moments and the ft value are practically determined at HF level. The phonons exert only a weak quenching action. They affect, instead, the quadrupole moments and $E2$ transitions. The core corrections are substantial but not sufficient to bring them close to the experimental values. The low-lying $E1$ transitions, connecting states of single particle nature, carry unrealistically large strengths. These results suggest that we need to enhance the amplitudes of the one-phonon components of the states of single particle nature and reduce their weights in the states of one-phonon nature.

A possible recipe for achieving this goal, thereby bridging the gap with experimental data, may consist in improving the HF description of the single particle spectra which amounts to improve the nucleon-nucleon potential as already advocated for even-even nuclei. In fact the levels or groups of levels above the Fermi surface are too far apart, especially as the energy increases, a common

featureof HF spectra derived from NN interactions [26, 97]. More compressed HF(B) level schemes would yield more compact TDA one-phonon spectra and, therefore,would enhance the particle to one-phonon coupling.

The need of improving the optimized two-body chiral potential $NNLO_{opt}$ is motivated by the fact that it produces too much attraction in medium and heavy mass nuclei. In fact, in the heavy even-even nuclei, we were forced to add a phenomenological repulsive density dependent term. This ad hoc prescription is certainly unsatisfactory. It might, nonetheless, offer some useful hints on how to proceed in order to derive the necessary corrections to $NNLO_{opt}$. The new optimized interaction $NNLO_{sat}$ [111], involving both two- and three-body components of NNLO, would be a possible solution. In this potential, in fact, two-nucleon and three-nucleon forces from chiral effective field theory are optimized simultaneously to low-energy nucleon-nucleon scattering data, as well as binding energies and radii of few-nucleon systems and selected isotopes of carbon and oxygen.

The positive parity states would be marginally affected by a more accurate HF level scheme. They would remain at too high energy. The analysis of their structure suggests that several particle-core states having mixed phonon structure are just above $\sim$ 11 MeV and those of two-phonon character above 14 MeV. If coupled to four phonons, few of these states are likely to intrude into the low-energy sector of the spectrum. On the ground of the heuristic arguments given above, the four phonons are expected to couple strongly to two phonons and, therefore, to push them down in energy thereby favoring the mixing among different n-phonon components.

The occurrence of (2p-2h) and/or (4p-4h) positive parity levels at low energy

in ^{16}O was predicted long ago in the pioneering work of Brown and Green [112] and ascertained quantitatively in a phenomenological shell model approach [113]. It is, therefore, mandatory to include at least four phonons for a satisfactory description of the full energy spectra and transitions in the two nuclei investigated here. Including four phonons is a difficult but not impossible task if we are allowed to resort to approximations analogous to the ones we made here for three phonons.

Different projects are now on going. Indeed, we are completing the calculations for ^{15}O and ^{15}N, within the hole-core version of the method, and soon we will study also heavier nuclei in the Ca region. Furthermore, the method has been formulated in the quasiparticle scheme, suited for nuclei with open shell core, and is being implemented numerically to neutron rich odd nuclei with an odd nucleon external to open shell cores.

The other project planned for the near future is the extension of the method to odd-odd nuclei with two particles external to a doubly magic core. This would allow us to investigate the spin-isospin excitations. Since our method allows calculations in very large spaces, it should be possible to evaluate the quenching action of many particle-hole high energy configurations on the GT transitions.

Appendix A

HFB canonical basis

This appendix describes the Block-Messiah-Zumino theorem. It defines the canonical basis adopted for solving the HFB problem. The Bogolyubov transformations in matrix form are given by

$$\begin{pmatrix} \beta \\ \beta^\dagger \end{pmatrix} = \mathscr{W}^\dagger \begin{pmatrix} c \\ c^\dagger \end{pmatrix} \tag{A.1}$$

where

$$\mathscr{W} = \begin{pmatrix} U & V^* \\ V & U^* \end{pmatrix}. \tag{A.2}$$

The Bloch-Messiah-Zumino (BMZ) theorem [114, 115], states that a unitary matrix W of the form (A.2) can always be decomposed as the product of three matrices

$$\mathscr{W} = \begin{pmatrix} D & 0 \\ 0 & D^* \end{pmatrix} \begin{pmatrix} \bar{U} & \bar{V} \\ \bar{V} & \bar{U} \end{pmatrix} \begin{pmatrix} C & 0 \\ 0 & C^* \end{pmatrix} \tag{A.3}$$

or

$$U = D\bar{U}C, \qquad V = D^*\bar{V}C, \tag{A.4}$$

where D and C are unitary matrices, and $\bar{U}$ and $\bar{V}$ are real matrices of the form

$$\bar{U} = \begin{pmatrix} 0 & & & & & & & & 0 & & \\ & \ddots & & & & & & & & & \\ & & u_1 & 0 & & & & & & & \\ & & 0 & u_1 & & & & & & & \\ & & & & \ddots & & & & & & \\ & & & & & u_n & 0 & & & & \\ & & & & & 0 & u_n & & & & \\ & & & & & & & 1 & & & \\ & & & & & & & & 1 & & \\ & 0 & & & & & & & & \ddots & \\ & & & & & & & & & & 1 \end{pmatrix} \tag{A.5}$$

$$\bar{V} = \begin{pmatrix} 1 & & & & & & & & & & & 0 & & \\ & \ddots & & & & & & & & & & & & \\ & & 1 & & & & & & & & & & & \\ & & & 0 & v_1 & & & & & & & & & \\ & & & -v_1 & 0 & & & & & & & & & \\ & & & & & & & & & & & & & \\ & & & & & & \ddots & & & & & & & \\ & & & & & & & & 0 & v_n & & & & \\ & & & & & & & & -v_n & 0 & & & & \\ & 0 & & & & & & & & & & 0 & & \\ & & & & & & & & & & & & \ddots & \\ & & & & & & & & & & & & & 0 \end{pmatrix}. \tag{A.6}$$

Thus, this theorem states that the HFB transformation is composed of three parts:

i) A unitary transformation D that defines the *canonical* basis

$$a_j^\dagger = \sum_i D_{ij} c_i. \tag{A.7}$$

ii) a special Bogoliubov transformation

$$\begin{aligned} \alpha_r^\dagger &= u_r a_r^\dagger - v_r a_r \\ \alpha_r &= u_r a_r^\dagger + v_r a_r \end{aligned} \tag{A.8}$$

which corresponds to the BCS transformation, and defined the canonical basis,

iii) a unitary transformation C

$$\beta_r^\dagger = \sum_r C_{ir} \alpha_i^\dagger \tag{A.9}$$

which transforms the qp operators among themselves. The theorem tells us that the general HFB transformation defining the qp operators $(\beta^\dagger, \beta)$ can be turned

into the simpler canonical BCS form defining the $(\alpha^{\dagger}, \alpha)$ operators by using an appropriate basis.

Appendix B

Cholesky decomposition

This appendix describes the Cholesky decomposition method, which allows to extract a subset of linearly independent states from a redundant basis.

If a square matrix **A** is symmetric and positive definite, it can be decomposed more efficiently using the Cholesky algorithm. This method decomposes the matrix as a product of a lower triangular matrix, **L**, and its transpose, $\mathbf{L}^T$

$$A = LL^T \tag{B.1}$$

writing it in component one gets that the diagonal elements of the lower triangular matrix, **L**

$$L_{ii} = \left(a_{ii} - \sum_{k=0}^{i-1} L_{ik}^2 \right)^{\frac{1}{2}} \tag{B.2}$$

and the off-diagonal matrix elements

$$L_{ji} = \frac{1}{L_{ii}} \left(a_{ij} - \sum_{k=0}^{i-1} L_{ik} L_{jk} \right)^{\frac{1}{2}} \tag{B.3}$$

This decomposition is extremely stable from a numerical point of view. Cholesky decomposition is often used for finding the matrix rank and determinant. In fact, once the symmetric and positive definite matrix, A, has been decomposed, its determinant is given by

$$det(\mathbf{A}) = det(\mathbf{L}) \times det(\mathbf{L}^T) \tag{B.4}$$

that is, from the product of the square of the diagonal term of $\mathbf{L}$, $(\prod_i L_{ii})^2$. The determinant can then be calculated on-line while doing the decomposition. If at the $(j+1)-th$ step of the decomposition the determinant is nullified, one has determined the matrix rank $r = j < n$.

Bibliography

[1] A. Bohr and B. R. Mottelson, *Nuclear Structure, Vol. II* (W. A. Benjamin, New York, 1975).

[2] W. Bothe and W. Gentner, Zeitschrift für Physik **106**, 236 (1937).

[3] G. Baldwin and G. Klaiber, Physical Review **71**, 3 (1947).

[4] G. F. Bertsch, P. F. Bortignon, and R. A. Broglia, Rev. Mod. Phys. **55**, 287 (1983).

[5] P. Bortignon, A. Bracco, and R. Broglia, *Giant resonances: nuclear structure at finite temperature* (1998).

[6] M. Harakeh and A. Van der Woude, *Giant resonances: Fundamental high-frequency modes of nuclear excitations* (2001).

[7] J. Sawicki, Phys. Rev. **126**, 2231 (1962).

[8] C. Yannouleas, M. Dworzecka, and J. Griffin, Nuclear Physics A **397**, 239 (1983).

[9] C. Yannouleas, Phys. Rev. C **35**, 1159 (1987).

[10] P. Papakonstantinou and R. Roth, Phys Rev. C **81**, 024317 (2010).

[11] D. Gambacurta, M. Grasso, and F. Catara, Phys. Rev. C **84**, 034301 (2011).

[12] D. Gambacurta, M. Grasso, V. De Donno, G. Co', and F. Catara, Phys. Rev. C **86**, 021304 (2012).

[13] E. Litvinova, P. Ring, and V. Tselyaev, Phys. Rev. C **78**, 014312 (2008).

[14] E. Litvinova, P. Ring, and V. Tselyaev, Phys. Rev. Lett. **105**, 022502 (2010).

[15] I. A. Egorova and E. Litvinova, Phys. Rev. C **94**, 034322 (2016).

[16] G. Colò and P. F. Bortignon, Nucl. Phys. A **696**, 427 (2001).

[17] G. Coló, H. Sagawa, and P. Bortignon, Phys Rev. C **82**, 064307 (2010).

[18] V. G. Soloviev, *Theory of Atomic Nuclei Quasiparticles and Phonons* (Institute of Physics Publishing, Bristol, Avon, 1992).

[19] F. Andreozzi, F. Knapp, N. Lo Iudice, A. Porrino, and J. Kvasil, Phys. Rev. C **75**, 044312 (2007).

[20] D. Bianco, F. Knapp, N. Lo Iudice, F. Andreozzi, and A. Porrino, Phys. Rev. C **85**, 014313 (2012).

[21] D. R. Hartree, Mathematical Proceedings of the Cambridge Philosophical Society **24**, 89 (1928).

[22] V. Fock, Zeitschrift für Physik **61**, 126 (1930).

[23] A. Messiah, *Quantum mechanics. vol. i.*. (1958).

[24] P. Ring and P. Schuck, *The Nuclear Many-Body Problem* (Springer, 1980).

[25] H. Hergert, P. Papakonstantinou, and R. Roth, Phys. Rev. C **83**, 064317 (2011).

[26] D. Bianco, F. Knapp, N. Lo Iudice, P. Veselý, F. Andreozzi, G. De Gregorio, and A. Porrino, J. Phys. G: Nucl. Part. Phys. **41**, 025109 (2014).

[27] D. Gambacurta, M. Grasso, and F. Catara, Phys. Rev. C **81**, 054312 (2011).

[28] D. Gambacurta, M. Grasso, and J. Engel, Phys. Rev. C **92**, 034303 (2015).

[29] F. Minato, Phys. Rev. C **93**, 044319 (2016).

[30] B. Schwesinger and J. Wambach, Physics Letters B **134**, 29 (1984).

[31] B. Schwesinger and J. Wambach, Nuclear Physics A **426**, 253 (1984).

[32] J. Dehesa, S. Krewald, and J. Speth, Phys. Rev. C **15**, 1858 (1977).

[33] P. Bortignon and R. Broglia, Nuclear Physics A **371**, 405 (1981).

[34] V. G. Soloviev, *Theory of Atomic Nuclei, Quasi-particle and Phonons* (CRC Press, 1992).

[35] N. Tsoneva, H. Lenske, and C. Stoyanov, Phys. Lett. B **586**, 213 (2004).

[36] N. Tsoneva and H. Lenske, Phys. Rev. C **77**, 024321 (2008).

[37] N. Tsoneva and H. Lenske, Phys. Rev. C **77**, 024321 (2008).

[38] A. P. Tonchev, S. L. Hammond, J. H. Kelley, E. Kwan, H. Lenske, G. Rusev, W. Tornow, and N. Tsoneva, Phys. Rev. Lett. **104**, 072501 (2010).

[39] R. Schwengner, R. Massarczyk, G. Rusev, N. Tsoneva, D. Bemmerer, R. Beyer, R. Hannaske, A. R. Junghans, J. H. Kelley, E. Kwan, et al., Phys. Rev. C **87**, 024306 (2013).

[40] G. Rusev, N. Tsoneva, F. Dönau, S. Frauendorf, R. Schwengner, A. P. Tonchev, A. S. Adekola, S. L. Hammond, J. H. Kelley, E. Kwan, et al., Phys. Rev. Lett. **110**, 022503 (2013).

[41] E. Litvinova and P. Ring, Phys Rev. C **73**, 044328 (2006).

[42] E. Litvinova, P. Ring, and D. Vretenar, Phys. Lett. B **647**, 111 (2007).

[43] E. Litvinova, P. Ring, V. Tselyaev, and K. Langanke, Phys. Rev. C **79**, 054312 (2009).

[44] E. Litvinova, B. Brown, D.-L. Fang, T. Marketin, and R. Zegers, Physics Letters B **730**, 307 (2014).

[45] D. Bianco, F. Andreozzi, N. Lo Iudice, A. Porrino, and F. Knapp, Phys Rev. C **85**, 034332 (2012).

[46] F. Knapp, N. Lo Iudice, P. Veselý, F. Andreozzi, G. De Gregorio, and A. Porrino, Phys. Rev. C **90**, 014310 (2014).

[47] F. Knapp, N. Lo Iudice, P. Veselý, F. Andreozzi, G. De Gregorio, and A. Porrino, Phys Rev. C **92**, 054315 (2015).

[48] G. De Gregorio, F. Knapp, N. Lo Iudice, and P. Veselý, Phys Rev. C **93**, 044314 (2016).

[49] C. Mahaux, P. F. Bortignon, R. A. Broglia, and C. H. Dasso, Phys. Rep. **120**, 1 (1985).

[50] L.-G. Cao, G. Coló, H. Sagawa, and P. Bortignon, Phys Rev. C p. 044314 (2014).

[51] Y. F. Niu, Z. M. Niu, G. Colò, and E. Vigezzi, Phys. Rev. Lett. **114**, 142501 (2015).

[52] G. Co', V. De Donno, M. Anguiano, R. N. Bernard, and A. M. Lallena, Phys Rev. C **92**, 024314 (2015).

[53] A. V. Afanasjev and E. Litvinova, Phys. Rev. C **92**, 044317 (2015).

[54] N. V. Gnezdilov, I. N. Borzov, E. E. Saperstein, and S. V. Tolokonnikov, Phys. Rev. C **89**, 034304 (2014).

[55] A. Cipollone, C. Barbieri, and P. Navrátil, Phys. Rev. Lett. **111**, 062501 (2013).

[56] B. R. Barrett, P. Navrátil, and J. P. Vary, Progress in Particle and Nuclear Physics **69**, 131 (2013).

[57] G. Hagen, T. Papenbrock, and M. Hjorth-Jensen, Phys. Rev. Lett. **104**, 182501 (2010).

[58] G. R. Jansen, J. Engel, G. Hagen, P. Navratil, and A. Signoracci, Phys. Rev. Lett. **113**, 142502 (2014).

[59] G. Hagen, T. Papenbrock, M. Hjorth-Jensen, and D. J. Dean, Rep. Prog. Phys. **77**, 096302 (2014).

[60] G. De Gregorio, F. Knapp, N. Lo Iudice, and P. Vesely, Phys. Rev. C **94**, 061301 (2016).

[61] G. De Gregorio, F. Knapp, N. Lo Iudice, and P. Veselý, Phys. Rev. C **95**, 034327 (2017).

[62] A. Ekström, G. Baardsen, C. Forssén, G. Hagen, M. Hjorth-Jensen, G. R. Jansen, R. Machleidt, W. Nazarewicz, T. Papenbrock, J. Sarich, et al., Phys. Rev. Lett. **110**, 192502 (2013).

[63] M. Goldhaber and E. Teller, Phys. Rev. **74**, 1046 (1948).

[64] H. Steinwedel and Z. Jensen, Naturforschung **5A** (1950).

[65] G. A. Bartholomew, Annual Review of Nuclear Science **11**, 259 (1961).

[66] S. Goriely, Physics Letters B **436**, 10 (1998).

[67] N. Paar, C. C. Moustakidis, T. Marketin, D. Vretenar, and G. A. Lalazissis, Phys. Rev. C **90**, 011304 (2014).

[68] N. Tsoneva, S. Goriely, H. Lenske, and R. Schwengner, Phys. Rev. C **91**, 044318 (2015).

[69] A. Leistenschneider, T. Aumann, K. Boretzky, D. Cortina, J. Cub, U. Datta Pramanik, W. Dostal, T. W. Elze, H. Emling, H. Geissel, et al., Phys. Rev. Lett. **86**, 5442 (2001).

[70] P. Adrich, A. Klimkiewicz, M. Fallot, K. Boretzky, T. Aumann, D. Cortina-Gil, U. D. Pramanik, T. W. Elze, H. Emling, H. Geissel, et al. (LAND-FRS Collaboration), Phys. Rev. Lett. **95**, 132501 (2005).

[71] K. Govaert, F. Bauwens, J. Bryssinck, D. De Frenne, E. Jacobs, W. Mondelaers, L. Govor, and V. Yu. Ponomarev, Phys. Rev. C **57**, 2229 (1998).

[72] N. Ryezayeva, T. Hartmann, Y. Kalmykov, H. Lenske, P. von Neumann-Cosel, V. Y. Ponomarev, A. Richter, A. Shevchenko, S. Volz, and J. Wambach, Phys. Rev. Lett. **89**, 272502 (2002).

[73] A. Zilges, S. Volz, M. Babilon, T. Hartmann, P. Mohr, and K. Vogt, Physics Letters B **542**, 43 (2002).

[74] T. Hartmann, M. Babilon, S. Kamerdzhiev, E. Litvinova, D. Savran, S. Volz, and A. Zilges, Phys. Rev. Lett. **93**, 192501 (2004).

[75] D. Savran, M. Babilon, A. M. van den Berg, M. N. Harakeh, J. Hasper, A. Matic, H. J. Wörtche, and A. Zilges, Phys. Rev. Lett. **97**, 172502 (2006).

[76] J. Endres, E. Litvinova, D. Savran, P. A. Butler, M. N. Harakeh, S. Harissopulos, R.-D. Herzberg, R. Krücken, A. Lagoyannis, N. Pietralla, et al., Phys. Rev. Lett. **105**, 212503 (2010).

[77] J. Endres, D. Savran, P. A. Butler, M. N. Harakeh, S. Harissopulos, R.-D. Herzberg, R. Krücken, A. Lagoyannis, E. Litvinova, N. Pietralla, et al., Phys. Rev. C **85**, 064331 (2012).

[78] V. Derya, D. Savran, J. Endres, M. Harakeh, H. Hergert, J. Kelley, P. Papakonstantinou, N. Pietralla, V. Yu. Ponomarev, R. Roth, et al., Phys. Lett. B **730**, 288 (2014).

[79] D. Negi, M. Wiedeking, E. G. Lanza, E. Litvinova, A. Vitturi, R. A. Bark,

L. A. Bernstein, D. L. Bleuel, S. Bvumbi, T. D. Bucher, et al., Phys. Rev. C **94**, 024332 (2016).

[80] F. C. L. Crespi, A. Bracco, R. Nicolini, D. Mengoni, L. Pellegri, E. G. Lanza, S. Leoni, A. Maj, M. Kmiecik, R. Avigo, et al., Phys. Rev. Lett. **113**, 012501 (2014).

[81] F. C. L. Crespi, A. Bracco, R. Nicolini, E. G. Lanza, A. Vitturi, D. Mengoni, S. Leoni, G. Benzoni, N. Blasi, C. Boiano, et al., Phys. Rev. C **91**, 024323 (2015).

[82] M. Krzysiek, M. Kmiecik, A. Maj, P. Bednarczyk, A. Bracco, F. C. L. Crespi, E. G. Lanza, E. Litvinova, N. Paar, R. Avigo, et al., Phys. Rev. C **93**, 044330 (2016).

[83] R. Mohan, M. Danos, and L. C. Biedenharn, Phys. Rev. C **3**, 1740 (1971).

[84] J. Piekarewicz, Phys. Rev. C **73**, 044325 (2006).

[85] E. G. Lanza, A. Vitturi, M. V. Andrés, F. Catara, and D. Gambacurta, Phys. Rev. C **84**, 064602 (2011).

[86] J. Piekarewicz, Phys. Rev. C **83**, 034319 (2011).

[87] D. Vretenar, Y. F. Niu, N. Paar, and J. Meng, Phys. Rev. C **85**, 044317 (2012).

[88] A. Klimkiewicz, N. Paar, P. Adrich, M. Fallot, K. Boretzky, T. Aumann, D. Cortina-Gil, U. D. Pramanik, T. W. Elze, H. Emling, et al. (LAND Collaboration), Phys. Rev. C **76**, 051603 (2007).

[89] J. Li, G. Colò, and J. Meng, Phys. Rev. C **78**, 064304 (2008).

[90] P. Papakonstantinou, H. Hergert, V. Yu. Ponomarev, and R. Roth, Phys. Rev. C **89**, 034306 (2014).

[91] Y. Kim and P. Papakonstantinou, The European Physical Journal A **52**, 176 (2016).

[92] N. Paar, D. Vretenar, E. Khan, and G. Coló, Report on Progress in Physics **70**, 691 (2007).

[93] N. Paar, J. Phys. G: Nucl. Part. Phys. **37**, 064014 (2010).

[94] X. Roca-Maza, X. Viñas, M. Centelles, B. K. Agrawal, G. Colò, N. Paar, J. Piekarewicz, and D. Vretenar, Phys. Rev. C **92**, 064304 (2015).

[95] D. Sarchi, P. Bortignon, and G. Coló, Phys. Lett. B **601**, 27 (2004).

[96] E. Litvinova, P. Ring, and D. Vretenar, Physics Letters B **647**, 111 (2007).

[97] R. Roth, N. Papakonstantinou, P.and Paar, H. Hergert, T. Neff, and H. Feldmeier, Phys Rev. C **73**, 044312 (2006).

[98] M. Waroquier, K. Heyde, and H. Vincx, Phys. Rev. C **13**, 1664 (1976).

[99] A. Günther, R. Roth, H. Hergert, and S. Reinhardt, Phys. Rev. C **82**, 024319 (2010).

[100] V. Isakov, K. Erokhina, H. Mach, M. Sanchez-Vega, and B. Fogelberg, The European Physical Journal A - Hadrons and Nuclei **14**, 29 (2002).

[101] B. Özel, J. Enders, P. von Neumann-Cosel, I. Poltoratska, A. Richter, D. Savran, S. Volz, and A. Zilges, Nucl. Phys. A **788**, 385 (2007).

[102] A. Tamii, I. Poltoratska, P. von Neumann-Cosel, Y. Fujita, T. Adachi, C. A. Bertulani, J. Carter, M. Dozono, H. Fujita, K. Fujita, et al., Phys. Rev. Lett. **107**, 062502 (2011).

[103] D. R. Tilley, C. M. Cheves, J. H. Kelley, S. Raman, and H. R. Weller, Nucl. Phys. A **636**, 249 (1998).

[104] E. Tryggestad, T. Baumann, P. Heckman, M. Thoennessen, T. Aumann, D. Bazin, Y. Blumenfeld, J. R. Beenec, T. A. Lewis, D. C. Radford, et al., Phys Rev. C **67**, 064309 (2003).

[105] E. Tryggestad, T. Aumann, T. Baumann, D. Bazin, J. R. Beene, Y. Blumenfeld, B. A. Brown, M. Chartier, M. L. Halbert, P. Heckman, et al., Phys. Lett. B **541**, 52 (2002).

[106] D. Tilley, H. Weller, and C. Cheves, Nuclear Physics A **564**, 1 (1993).

[107] J. Ahrens, H. Borchert, K. Czock, H. Eppler, H. Gimm, H. Gundrum, M. Kröning, P. Riehn, G. S. Ram, A. Zieger, et al., Nuclear Physics A **251**, 479 (1975).

[108] J. W. Jury, B. L. Berman, D. D. Faul, P. Meyer, and J. G. Woodworth, Phys Rev. C **21**, 503 (1980).

[109] H. Hergert, S. K. Bogner, T. D. Morris, S. Binder, A. Calci, J. Langhammer, and R. Roth, Phys. Rev. C **90**, 041302(R) (2014).

[110] G. De Gregorio, J. Herko, F. Knapp, N. Lo Iudice, and P. Veselý, Phys. Rev. C **95**, 024306 (2017).

[111] A. Ekström, G. R. Jansen, K. A. Wendt, G. Hagen, T. Papenbrock, B. D. Carlsson, C. Forssén, M. Hjorth-Jensen, P. Navrátil, and W. Nazarewicz, Phys. Rev. C **91**, 051301 (2015).

[112] G. E. Brown and A. M. Green, Nucl. Phys. **75**, 401 (1966).

[113] W. C. Haxton and C. Johnson, Phys. Rev. Lett. **65**, 1325 (1990).

[114] C. Bloch and A. Messiah, Nuclear Physics **39**, 95 (1962).

[115] B. Zumino, Journal of Mathematical Physics **3**, 1055 (1962).